Evaluating key properties of carbon materials as cathodes for the electrogeneration of hydrogen peroxide

M. Muñoz-Morales, A. Ramírez, Aurelien Cañizares, J. Llanos, Conchi Maria Concepcion Ovin Ania

Evaluating key properties of carbon materials as cathodes for the electrogeneration of hydrogen peroxide

M. Muñoz-Morales[1,2]*, A. Ramírez[2], Aurelien Cañizares[1], J. Llanos[2], Conchi Ania*[1]

[1] CEMHTI, CNRS (UPR 3079), Université d'Orléans, 45071 Orléans, France

[2] Chemical Engineering Dept., Faculty of Chemical Sciences & Technologies, University of Castilla La Mancha, Campus Universitario s/n 13071 Ciudad Real, Spain

* corresponding authors: martin.munoz@uclm.es; conchi.ania@cnrs-orleans.fr; Tel.: +33 238 25.55.13

Carbon, Volume 210, 15 June 2023, 118082

https://doi.org/10.1016/j.carbon.2023.118082

Abstract. Twenty two carbon materials of different origins (e.g., graphite, graphene, carbon black, hydrochars, activated carbons, carbon nanotubes and nanofibers) and with varied physicochemical characteristics (e.g., electrical conductivity, structural order, surface functionalization, porosity) were investigated as cathodes in the electrochemical production of hydrogen peroxide. A screening of the electrocatalytic performance was carried out in 0.2 cm^2 (inks casted on a glassy carbon) and 4 cm^2 electrodes (Toray paper). The highest H_2O_2 production yields were obtained for carbon nanotubes and carbon nanofibers, outperforming common carbon benchmarks for this application -i.e., carbon black, carbon felt-. Furthermore, a good catalytic activity was obtained with low-cost and disordered carbon cathodes with moderate electrical conductivity and density of structural defects (e.g., nanoporous carbons), both in terms of overall production rate, selectivity and energy consumption. Data also revealed that the H_2O_2 production yield and the faradaic efficiency are closely related to the structural parameters of the carbon materials (i.e., density of structural defects), rather than to the electrical conductivity, composition or porous features. An A_D/A_G threshold value of 1.5 can be used to discriminate the electrocatalytic activity of carbon cathodes for the production of H_2O_2 through a 2e-ORR, in terms of high production rates and good faradaic efficiencies.

Keywords: carbon cathodes, electrical conductivity, hydrogen peroxide, Toray paper, structural defects.

1. Introduction

Hydrogen peroxide is an oxidizing chemical widely used in a large number of strategic productive sectors such as the paper and pulp industry, chemical synthesis, food and beverages, water treatment, textiles and laundry, and electronics among others [1]. Furthermore, hydrogen peroxide is a potential energy carrier and can be used in one-compartment H_2O_2 fuel cells to generate electricity [2, 3]. The significance of the global hydrogen peroxide market is evidenced by the over 5 million tons annual production in 2021 (market dominated by the chemical synthesis and the paper and pulp industries), and an expected compound annual growth rate (CAGR) index over 3% in the next five years [4].

Current industrial production is mostly carried out through the anthraquinone autoxidation process [5-8], an energy-intensive and complex one with a wide number of technological drawbacks (i.e., large waste production, low efficiency, mass transfer limitation, excessive solvent use) [9]. These issues have triggered the research efforts to develop more efficient, safe and green methods for the synthesis of hydrogen peroxide (catalytic, enzymatic, photocatalytic, electrochemical). Among them, the production of H_2O_2 from the electrochemical reduction of oxygen has become an interesting alternative, as it can be operated at room temperature and atmospheric pressure and allows on-site operation, avoiding costs and risks associated to its transport and storage. The electrochemical production of H_2O_2 relies on the 2-electron oxygen reduction reaction (2e-ORR). This reaction is typically limited by low oxygen solubility in aqueous electrolytes at room temperature, and depends to a large extent on the cathode material [10]. Owing to their unique structural and electronic properties, many carbon materials have been investigated for this application, such as graphite felts [11, 12], reticulated vitreous carbon [13], activated carbon [14, 15], carbon paper [16], carbon felt [17]. Compared to noble-metal-based electrocatalysts, carbon-based materials offer the advantage of their low cost, availability, good conductivity, as well as the possibility to modulate their characteristics (e.g., porosity, surface defects, composition) to favor the selectivity towards the 2e-ORR pathway [18-20]. The most commonly used carbon cathodes for the electrogeneration of H_2O_2 are graphites, carbon blacks and carbon felts [21-23]. The latter has several disadvantages related to the cost and poor performance in pilot scales-up flow reactors due to their flexibility [24-26]. In the case of carbon black, low faradaic efficiencies are usually obtained when large electrodes are used due to oxygen transfer limitations related to their solubility in water [27, 28], although this is

counterbalanced by their low cost and a high electronic conductivity. Nevertheless, other researchers testing different carbon matrices without O_2 diffusion problems indicate that if the ORR onset is shifted towards more positive potential the energy consumption is lower and hence the faradaic efficiency is higher [29, 30].

Other carbon materials have also been largely investigated as cathodes for the electrogeneration of H_2O_2 [21, 31, 32]; however, there is a lack of understanding of the correlation between the physicochemical and structural characteristics that includes a wide spectrum of different types of carbon materials and their electrocatalytic activity for the generation of H_2O_2 using 4 cm^2 electrodes. For instance, it has been reported that the porosity of the carbon cathodes influences the mass transfer rate of the ORR species (being that of H_2O_2 larger than that of O_2) as well as the strength of the oxygen adsorption sites -i.e., binding energy towards the catalyst's surface- favoring the 2e- ORR pathway (avoiding further reduction to water) [33]. Surface functionalization of the carbon cathodes has also been reported to have a large impact on the electrocatalytic activity and selectivity for the 2e-ORR [34-36]. In this regard, a large number of studies have reported the beneficial effect of heteroatom doping of the carbon cathodes on their H_2O_2 production [20, 37, 38]. However, owing to the complexity of achieving selective surface modification of carbon materials, the role of the individual functional groups and their synergy in the electrocatalytic performance remain rather unknown. On the other hand, the role of the electric conductivity of the carbons is scarcely addressed; carbon materials are typically considered good conductors, although such characteristic varies considerable depending on the type of carbon material (e.g., from highly conductive graphite or graphene to poor conductive amorphous porous carbons).

Although there are other important factors for an efficient electrochemical production of H_2O_2 [23, 39, 40] specially when high surface electrodes are studied, a proper selection of the carbon cathode considering the physicochemical, structural and electrochemical parameters of the carbon material is of great relevance for this application.

Thus, the aim of this work was to perform a screening of carbon materials with varied physicochemical features as cathodes for the electrochemical production of H_2O_2. The portfolio of carbon materials ranged from graphite, graphene and derivatives, chars, activated carbons, carbon nanotubes and carbon nanofibers. They have been chosen based on their differences in surface chemistry, structural order, porosity and electrical conductivity; the aim is to clarify the role of these descriptors in the electrochemical production of H_2O_2. Furthermore, the electrocatalytic performance was measured on

relatively large cathodes (i.e., 2 x 2 cm^2), higher than most studies from the literature reporting the adequateness of carbon materials for this application (i.e., a few mm^2). This is important as it demonstrates the feasibility of large dimension cathodes for the electrochemical production of H_2O_2.

2. Experimental

2.1. Reagents

Sodium sulfate, sulfuric acid, PTFE (60% emulsion), 2-methyl propanol, 5%(v/v) Nafion® 117 solution and potassium titanium oxide oxalate dihydrate were purchased to Sigma-Aldrich. Polyvinylidene fluoride (PVDF) and N-Methyl-2-pyrrolidone were purchased to Merck. All aqueous solutions were prepared with Milli-Q water (18.2 MΩ cm).

2.2 Carbon materials

A series of carbon materials was used for the fabrication of the cathodes, including graphite, carbon black, graphene and derivatives, carbon nanotubes, petroleum coke, and nanoporous carbons. They were selected based on their different structural, porous and physicochemical properties. Details and nomenclature of the samples are compiled in Table 1. A complete characterization of the materials can be found in the Electronic Supplementary Information (Tables S1, S2, Fig. S1-S3).

Table 1. Nomenclature and selected characteristics of the carbon materials used as anodes in the electrocatalytic assays for the production of hydrogen peroxide.

Nomenclature	Characteristics
Gra	Graphite, commercial, supplied from Sigma Aldrich
CB	Carbon black, commercial, Superior Graphite (USA)
FLG	Few layers graphene, obtained by plasma [41]
GO	Graphene oxide, commercial, Graphenea (Spain)
rGO	Reduced graphene oxide, commercial, Graphenea (Spain)
CNF	Carbon Nanofibres, commercial, Antolin Group (Spain)
CNT	Multiwalled Carbon Nanotubes, commercial, Nanocyl (Belgium)

CNT-ox	Oxidized Multiwalled Carbon Nanotubes, commercial, Nanocyl (Belgium)
CFelt	Carbon Felt, commercial, Mersen
PCC	Char derived from delayed petroleum coke (900ºC under N_2 for 1 hour)
PCKOH	Nanoporous carbon obtained from KOH activation of petroleum coke (ratio 1:1) at 700ºC f under N_2 for 1 hour
NPQ	Nanoporous carbon, commercial (Aquasorb 2000, Jacobi Carbons), bituminous coal, steam activation [42, 43]
NPQgra	Sample NPQ (see below) graphitized at 2400ºC
NPB	Nanoporous carbon, chemical H_3PO_4 activation of biomass [42]
NPBH	Nanoporous carbon; sample NPB treated at 850 °C under inert atmosphere for 30 min to remove surface functionalities.
NPPW	Nanoporous carbon obtained from CO_2 activation of plastic waste at 925 °C, up to a burn-off of 34% [44]
NPBKK	Nanoporous carbon, commercial (BKK-100), bituminous coal, physical activation
NPcomp	Nanoporous carbon xerogel/carbon black composite (85:15 wt.%) [45]
HSU	Sucrose-derived hydrochar prepared at 180 °C [46]
HSU250	Sample HSU treated at 250 °C under inert atmosphere for 30 min to remove surface functionalities
HSU500	Sample HSU treated at 500 °C under inert atmosphere for 30 min to remove surface functionalities
HSU1000	Sample HSU treated at 1000 °C under inert atmosphere for 30 min to remove surface functionalities

2.3 Electrochemical Characterization

A preliminary electrochemical characterization of the carbon powders was carried out using linear seep voltammetry (LSV) technique and a glassy carbon electrode (GCE, 5.0 mm diameter, Goodfellow, UK) as support. LSVs were obtained via a potential sweep from +0.2 to -1.2 V vs. SCE at a scan rate of 10 mV s^{-1}. The GCE was previously polished using alumina (ca. 1.0, 0.3 and 0.05 μm) water suspensions. Inks of the carbon materials were prepared by suspending the carbon powders in 2-methyl propanol (10 mg/mL), adding an adequate volume of 20 wt.% nafion aqueous solution to reach a final concentration of ca. 5 wt.% nafion vs the weight of solid residue. The inks were sonicated for 45 min and then 5 μL was drop-casted onto the polished GCE (final loading of 128 μg cm^{-2}), and dried at 80ºC in air. The electrode films were labelled as X/GC, where X refers to the carbon materials used for the preparation of the inks. LSVs were recorded by a potentiostat (BioLogic) at a scan rate of 10 mV s^{-1} in a three-electrode configuration; the prepared X/GC electrodes were used as working electrode,

a graphite rod (ca. 0.385 cm^2) as counter and a saturated calomel electrode (SCE) as reference electrode. LSVs were also carried out in a rotating ring-disk electrode (RRDE-3A, ALS, Japan) constituted by a 3 mm diameter glassy carbon disk and a Pt ring, in O_2-saturated 0.050 M Na_2SO_4 electrolyte. A similar three-electrode cell configuration was used, with the RRDE as working electrode, a graphite rod as counter electrode and an Ag/AgCl reference electrode (scan rate of 5 mV/s; rotation speed (ω) between 500-5000 rpm). About 20 μL of the inks of the carbon materials were drop-casted on the glassy carbon disk (loading 0.4 mg/cm^2). The number of electrons transferred during ORR and the H_2O_2 yield were determined from the measured disk and ring currents. Further details are in the supplementary information file.

Contact angles were measured to determine wetting behaviour of the electrodes. Measurements were performed based on the sessile drop method, using 2 μl drops of deionised water deposited on the samples with a micropipette in a Digitrop (GBX) instrument. The contact angle was measured after stabilization of the water droplet in contact with the material surface. Averages of three independent measurements were registered for each sample.

2.4 Electrocatalytic H_2O_2 production

For the electrocatalytic assay for hydrogen peroxide generation, a 2 x 2 cm^2 Toray carbon paper® (TGPH-120, thickness 0.19 mm) was used as electrode substrate. Before applying the catalytic inks, the Toray papers was ultrasonicated for 30 min as reported elsewhere [47]. The carbon inks were prepared by suspending ca. 1 mg/mL of carbon powders and 50 mg/mL of PTFE (60% emulsion) in 2-methyl propanol, and sonicated for 15 minutes. The Toray papers were immersed in the ink, and sonicated for 15 min; then, the electrodes were dried in an oven at 80ºC for 24 hours to remove the excess of solvent. After drying, the electrodes were weighted to determine the loading coverage (Γ) in mg of carbon per cm^2, reaching average values ranging from 0.3-0.5 mg cm^2 for all prepared inks. Commercial carbon felt (with and without PTFE coating) was also tested as cathode material for comparison purposes.

The production of H_2O_2 was performed in an undivided cell (0.1 L) at room temperature and atmospheric pressure, using 0.05 M Na_2SO_4 at pH 6.5 (adjusted using 0.05 M H_2SO_4) as electrolyte. The 2 x 2 cm^2 Toray papers with the catalytic inks were used as cathode, and a graphite rod as anode (active surface 4.2 cm^2). The electrolyses were done in a potentiostatic mode, with an applied potential of -0.9 V using

potentiostat/galvanostat (Biologic). This potential was selected to assure the production of hydrogen peroxide in the electrodes (confirmed by a colorimetric method), while the potentiostatic mode was preferred to prevent high currents through the electrodes (due to their differences in conductivity, Table S2). The distance between the anode and cathode was fixed at 1 cm. A continuous supply of oxygen was applied by bubbling air; the solution was continuously stirred (300-400 rpm) using a magnetic bar to ensure a homogenous distribution of oxygen as reactant. The control electrolysis under a continuous flow of He to assure the absence of oxygen were also recorded. Prior starting the electrochemical treatment, the electrodes were immersed in the electrolyte (wetting) for 30 min under stirring. At time intervals, aliquots of 1 mL were taken for analyzing the concentration of H_2O_2. The concentration of H_2O_2 was measured by following the concentration of the complex formed between H_2O_2 and Ti(IV) measuring the absorbance at 408 nm on a UV-Vis spectrophotometer (Shimadzu) [48]. The nomenclature of the 2 x 2 cm^2 electrodes was X/TP, where X refers to the carbon materials used and TP stands for the Toray paper support.

Applied electric charge was used as a measure of the quantity of electricity supplied to the electrodes with the time and referred to the volume of solution. This parameter helps us to differentiate performance of electrodes according with the total power consumed. The applied electric charge (Q) was calculated as follows:

$$Q = \frac{I * t}{V} \qquad (1)$$

where I is the external current (A) at the applied voltage, t the time (s) and V the volume of the whole tank (L).

The faradaic efficiency (FE) of H_2O_2 production was calculated as follow [49]:

$$FE\ (\%) = \frac{n \cdot F \cdot [H_2O_2] \cdot V}{\int_0^t I \cdot dt}\ x\ 100 \qquad (2)$$

where n is the number of electrons transferred for ORR to H_2O_2, F the Faraday Constant (96486 C/mol), $[H_2O_2]$ is the concentration of H_2O_2 (mol/L), V the bulk liquid volume (L) in the reactor, I the external current according with the voltage chosen (A) and t the time (s).

The energy consumption (KWh/m^3) was calculated as [50]:

$$Energy\ consumption = \frac{U \cdot I \cdot t}{V} \qquad (3)$$

where U is the cell voltage (V), I is the current (A), V is the volume of the solution (m^3) and t is the time (h).

2.5. Characterization and Data Analysis

The selected carbon materials were thoroughly characterized using various techniques (e.g., gas adsorption isotherms, elemental analysis, Raman spectroscopy). Details of the experimental protocols are shown in the Supplementary Information File (Tables S1 and S2, Fig. S1-S3). A hierarchical cluster analysis method was used to analyze Raman data, following Ward's clustering algorithm (minimum variance method) and the Euclidian distance measure to generate a dendrogram using a script programmed in Phyton with Scipy library selecting *linkage function* and choosing the *Ward* method [51, 52]. The hierarchical cluster analysis was performed on the full Raman spectrum.

3. Results & discussion

3.1 Portfolio of carbon materials

A series of carbon materials with different physicochemical features were selected for this study, aiming to correlate their electrocatalytic activity towards the generation of H_2O_2 with the characteristics of the carbon (structural order, porosity, surface defects, composition and electrical conductivity). The carbon materials were characterized using various techniques (see Supplementary Information File); these properties are herein discussed in general terms.

Fig. 1 shows a selection of physicochemical properties of the studied carbon materials; namely composition and electric conductivity and a hierarchical cluster analysis of Raman data. The analysis of these properties (see discussion below) allowed us to classify the studied carbons in four groups, according to similarities in the structure, composition and electrical conductivity. This arbitrary classification will serve as a guide for the discussion on the electrocatalytic performance in the following sections.

- Group I (graphite, graphene, carbon black and graphitized carbon): low H/C and O/C ratios, high conductivity and high structural order;
- Group II (nanotubes, nanofibers, felt): low O/C and varied H/C ratio, high conductivity and moderate structural order;
- Group III (nanoporous carbons): low O/C and varied H/C ratio, moderate conductivity and low structural order;

Group IV (oxidized carbons): high O/C and H/C ratios, very low electrical conductivity, and high structural disorder.

The Van Krevelen diagram of the carbons shown in Fig. 1.a and 1.b provides an overview of the origin and compositional evolution (i.e., thermal history) of the carbons according to their atomic H/C and O/C ratios; this representation -frequently applied to biomass, hydrocarbons and fossil fuels-, allows classifying the studied carbons according to the aromaticity of the carbon atoms (H/C ratio) and the extent of surface functionalization (O/C ratio). Note that the carbons selected in this study cover a wide range of parameter space in the van Krevelen diagram.

Low H/C and O/C ratios are indicative of a high degree of aromaticity and low polarity, typically associated to carbon materials with high electrical conductivity. At converse, high H/C and O/C ratios are indicative of lower aromaticity of the carbon materials due to the surface functionalization, as well as of a high density of defects and low conductivity. This trend agrees with the electrical conductivity values obtained using the 4-probes method shown in Fig. 1.c (see also Table S1).

Regarding structural properties, the hierarchical cluster analysis of Raman data shown in Fig. 1.d shows four clusters with statistically large structural dissimilarities. A clear correlation was observed between those clusters and the functionalization and conductivity of the carbons. As an example, the first cluster (highlighted in green) is composed of samples graphite, graphene, carbon black and graphitized carbon, which are characterized by a high structural order but also low functionalization and high conductivity. A second cluster (highlighted in blue) is formed by samples with moderate structural order, along with low O/C and high conductivity. The last two clusters are composed of the carbons with a high functionalization and poor conductivity.

This classification will be used as a guide for the discussion on the electrocatalytic performance of the carbons in the following sections.

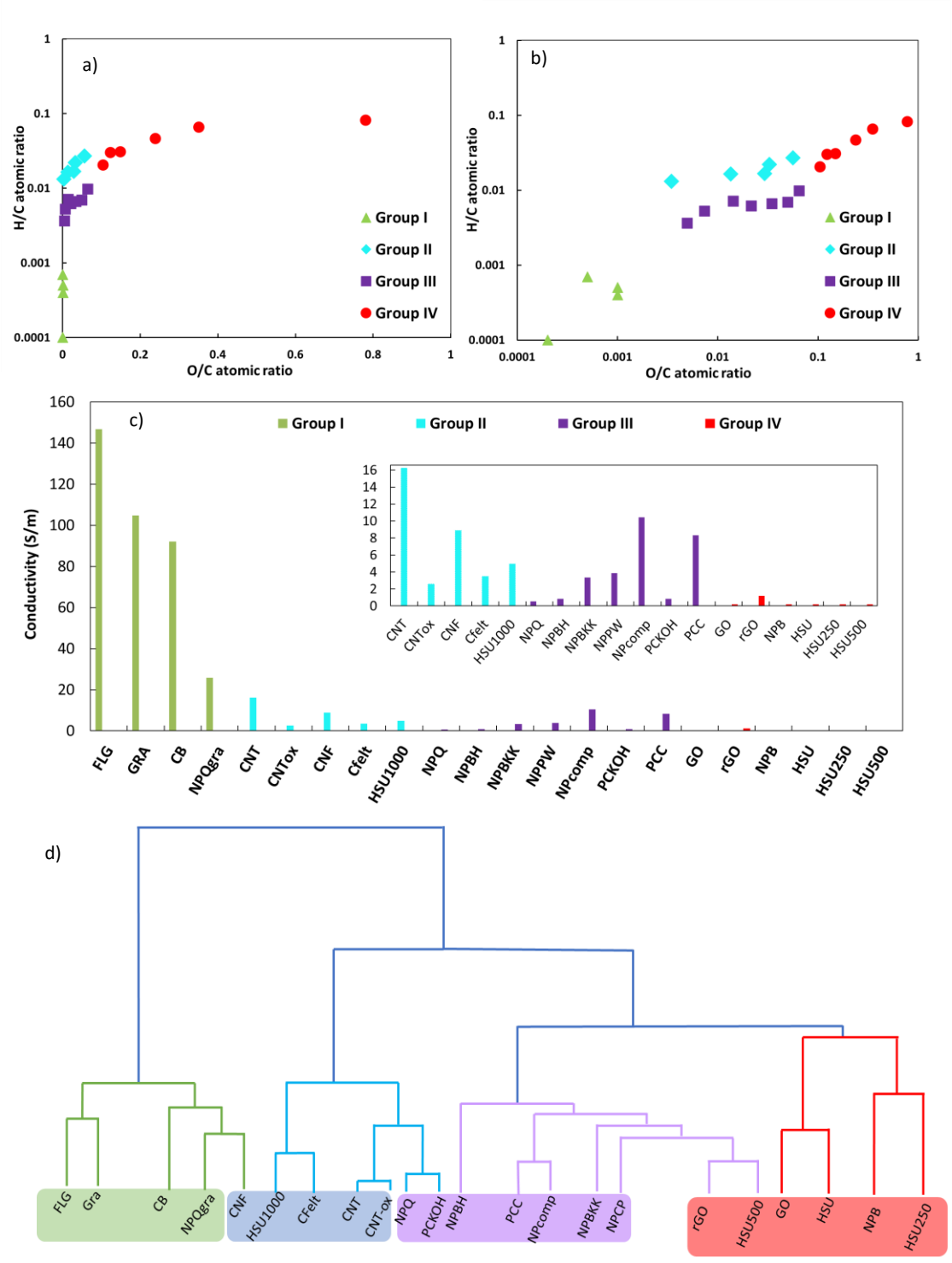

Fig. 1. Van Krevelen diagram for the selected carbon materials; data is shown in (a) linear and (b) logarithmic scale for clarity of comparison; (c) electrical conductivity of the carbon materials measured by the 4-probe method (inset accounts for a magnification of the scale); (d) Dendrogram representation resulting from the hierarchical cluster analysis of the full Raman spectra using Ward's algorithm.

3.2. Pre-screening of the electrocatalytic activity in a glassy carbon support

An initial pre-screening of the electrocatalytic activity of the selected carbons for the production of hydrogen peroxide was examined by Linear Sweep Voltammetry (LSV) in 0.05 M sodium sulphate on a 5 mm diameter glassy carbon support. The LSV curves were recorded in both O_2-saturated and He-saturated electrolyte by continuously bubbling air or helium in the electrochemical cell (before and during the analysis). This allowed determining the net current density for each electrode (i.e., iO_2 - iHe).

Fig. 2a shows the LSV of electrode CB/GC as a representative example of the studied materials; the LSV curves of the complete series of carbons are shown in Fig. S4. As seen, the curve in O_2-saturated electrolyte showed a marked cathodic wave with an onset potential (E_{onset}) at *ca*. -0.6V vs SCE, and a second change in the slope above -1 V *vs* SCE. The first wave is attributed to the ORR, following either a 4- or a 2-electron transfer mechanism, as indicated in the following competing reactions (stoichiometry shown for atmospheric pressure and acidic pH conditions):

$$O_{2(g)} + 4\,H^{+}_{(aq)} + 4\,e^{-} \rightarrow 2H_2O_{(aq)}\; E^0 = 1.23\;(vs\;RHE) \qquad (r1)$$

$$O_{2(g)} + 2\,H^{+}{}_{(aq)} + 2e^{-} \rightarrow H_2O_{2(aq)}\;\; E^0 = 0.70\;(vs\;RHE) \qquad (r2)$$

The second wave at higher onset potentials is due to the Hydrogen Evolution Reaction (HER) that occurs in parallel in the cathode (r3):

$$2\,H_2O\;(aq) + 2e^{-} \rightarrow H_2\;(g) + 2\,OH^{-}\;(aq)\;E^0 = 0.82\;(vs\;RHE) \qquad (r3)$$

It should be mentioned that carbon materials are typically good electrocatalysts for the HER but the choice of the experimental conditions (e.g., availability of oxygen in solution, electrolyte, applied potential) can contribute to suppress this reaction [53] and enhance the electrogeneration of H_2O_2 via $2e^-$ORR.

Fig. 2b,c show the values of the onset potential and the net electric current density evaluated at -0.9 V vs SCE for all the studied carbons. This potential value corresponds to the plateau of the first cathodic wave, and it was chosen as it allows the electrogeneration of H_2O_2 while minimizing the HER. As seen, current densities in the O_2-saturated electrolyte were higher than those in He-saturated environment for all the

studied carbons. This confirms the electrocatalytic activity of the electrodes for the reduction of oxygen to H_2O_2 at this potential. The formation of hydrogen peroxide was confirmed by a colorimetric method upon direct measurement in the electrolyte (see experimental section) for all the studied carbons. A RRDE was also used to confirm the electrocatalytic activity of the carbons towards the preferential reduction of oxygen through the formation of H_2O_2. Figure S5 shows the ring and disk currents recorded for selected carbons representative of the four studied groups. Significant oxidation currents were recorded in the Pt-ring electrode at sufficiently negative potentials due to the oxidation of H_2O_2 to O_2. Maximum oxidation currents were obtained at potentials above of -0.9V for all the samples, corresponding to a number of electrons between 1.9-2.3 and calculated H_2O_2 current efficiencies over 70%.

The onset potential values for the ORR varied between -200 and -600 mV *vs* SCE for all the carbons (most values above -600 mV *vs* SCE). Only for carbons NPBH and PCKOH an onset value could not be clearly identified in the LSV curves; both carbons displayed certain electrocatalytic activity for the production of H_2O_2 when the electrolysis was carried out in bigger electrodes as it will be discussed in the next section.

For comparison purpose, the performance of the carbons in terms of current density was compared at an applied potential of -0.9 V vs. SCE. This value was negative enough to assure the production of hydrogen peroxide in all the studied samples (confirmed by a colorimetric method), with rather constant current values. It was also the potential chosen for the electrolysis in 4 cm^2 electrodes (next section). Overall, no clear correlation was observed between the onset potential values and the characteristics of the four groups of carbons. In general terms, low E_{onset} values were obtained for groups I and II (characterized by low H/C and O/C ratios and high electrical conductivity), with the exception of graphite and carbon black that presented values similar to those of carbon in groups III and IV (carbons with much lower oxidation extent, and electrical conductivities of at least an order of magnitude lower).

Carbons from groups I and II presented (on average) among the highest net current densities (ca. 0.25-0.5 mA/cm^2), pointing out the important role of the electrical conductivity of the cathodes.

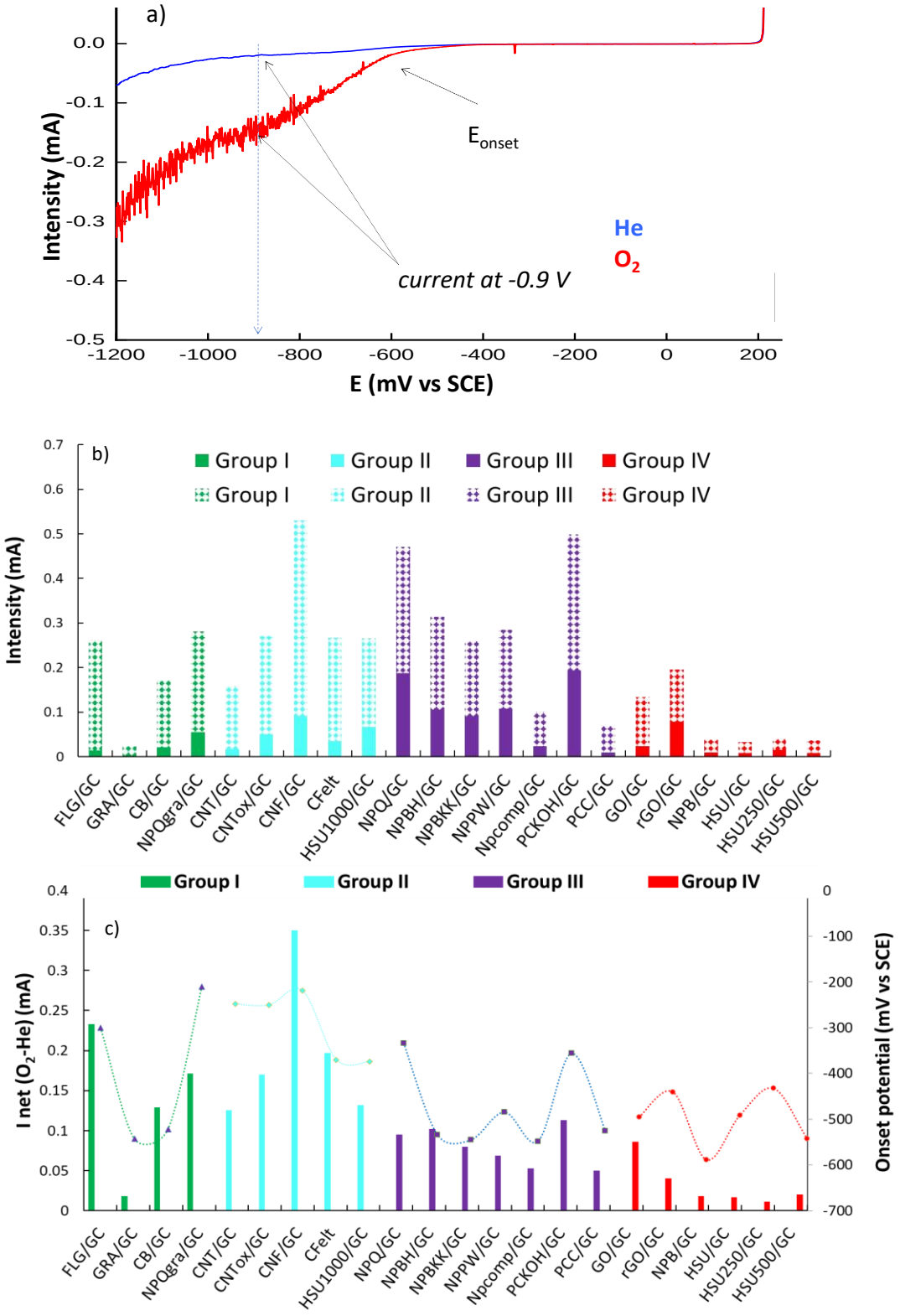

Fig. 2. a) Example of LSV curve of electrode CB/GC in 0.05 M Na_2SO_4 in He-saturated (blue) and O_2-saturated (red) conditions; b) current densities from the LSV curves at -0.9 V vs SCE in He-saturated (filled bars) and O_2-saturated (pattern bars) conditions; c) net current density (iO_2 - iHe) and onset potential values. Working electrode support: glassy carbon (5 mm); counter electrode: graphite rod; reference electrode: saturated calomel (SCE).

Similarly, the graphitization of carbon NPQ from Group IV (to render sample NPQgra) resulted in an increase in the net current density, due to the enhancement in conductivity. However, the net current density of carbons from Group III was comparable to that of sample CNT and CB (groups II and I, respectively), and significantly higher than that of sample GRA in Group I (all of them showing much higher electrical conductivities). This indicates that the conductivity of the cathodes -even though an important parameter-, is not the only parameter governing the electrocatalytic production of H_2O_2.

Regarding surface functionalization, different trends were observed. The presence of O-groups improved the electrocatalytic activity of samples CNT and rGO (compared to CNTox and GO, respectively), despite the considerable loss in electrical conductivity upon functionalization. This would be in agreement with the abundant literature reporting the beneficial role of heteroatom doping on the electrocatalytic activity of carbon materials in the 2e-ORR [20]. In contrast, a similar trend was not observed for the materials of group IV derived from a hydrochar (samples HSU, HSU250, HSU500 and HSU1000) or for carbons NPB and NPBH. The electrocatalytic of sample HSU (oxygen content ca. 20 wt.%) increased upon thermal annealing of the sample to remove the oxygen functionalities. A similar behavior would explain the low performance of sample NPB compared to NPBH treated at 800ºC. This points out that the gained in conductivity upon the thermal treatment becomes a more critical parameter than the loss of wettability/ hydrophilicity of the electrodes.

The latter was corroborated by the similar wetting behavior of all the studied electrodes, as inferred from the contact angle measurements (Fig. S6, S7). In this regard, it is well known that the surface wettability of electrodes can be tuned upon the incorporation of a binder in the composition of the inks [54] As a result, all the electrodes presented a marked hydrophobic character, despite the different hydrophobic/hydrophilic character of the pristine carbon materials (Table S2). Such hydrophobicity has been demonstrated to provide enough oxygen to the electrocatalytic sites to favor the two-electron ORR activity for H_2O_2 production, through the formation of triple-phase (oxygen gas−electrolyte−electrode) contact points [55].

The presence of structural defects in the carbons seems to play a key role in the electrocatalytic activity determined by LSV, as evidenced in Fig. 3 showing the correlations with the structural parameters obtained from the analysis of Raman data using Sadezky'5 bands mode [56]. As seen, higher net current densities where obtained

for the carbons with high A_{D1}/A_G ratio and low full-width at medium high of band D; both parameters are strongly related with the structural order of the carbons and the presence of in-plane defects [57]. With the exception of one sample (graphite), the lowest net current densities were obtained for the carbons from Groups III and IV, characterized by A_{D1}/A_G between 1.5-3. Similarly, both groups of carbons present FWMH values for the D band above 100. The similar correlation of the current density with the electrical conductivity (Fig. 3c) rendered a less conclusive trend, with similar current densities for carbons in Groups III and II with different electrical conductivity (as discussed above). Thus, it appears that threshold values of both structural parameters can be used to describe the electrocatalytic performance of the cathodes in terms of current density (a lower impact was observed for the onset potential, Fig. S5). Further correlations will be made based on the electrocatalytic performance of large electrodes (4 cm^2) in the next section.

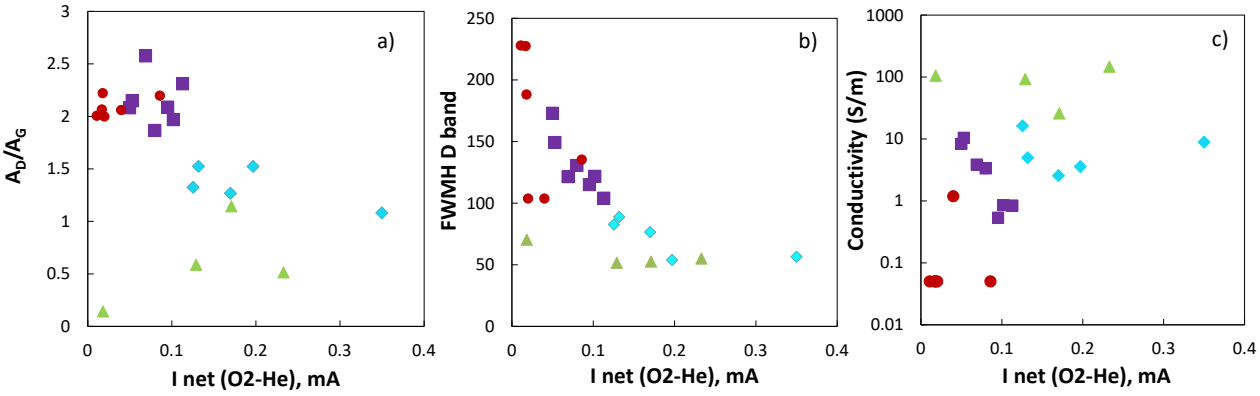

Fig. 3. Correlation between a) the ratio A_{D1}/A_G of Raman spectra, b) the FWHM of D band and c) the electrical conductivity vs the net current density of the studied carbons obtained at -0.9 vs SCE. Working electrode: glassy carbon (5 mm); counter electrode: graphite rod; reference electrode: saturated calomel (SCE).

3.3. Electrocatalytic H_2O_2 production of carbon-based materials supported in a 4 cm^2 carbon paper

The electrochemical production of H_2O_2 was evaluated in 4 cm^2 electrodes (to disregard limiting factors of low surface area electrodes related to limited quantification of H_2O_2). Constant air bubbling in the vicinity of cathode was applied to minimize any mass-transfer issues of dissolved oxygen at the interface electrode/electrolyte [27, 48]. For this, porous Toray paper was used as support for the fabrication of the cathodes (with

the exception of the carbon felt that was used as-received). As indicated in the experimental section, the electrocatalytic assays were carried out in potentiostatic mode at -0.9 V vs SCE to selectively promote the electrochemical reduction of O_2 to H_2O_2.

Fig. 4 shows the evolution of H_2O_2 over time and *versus* the applied electric charge for all the studied carbons. Data is expressed in ppm H_2O_2 (absolute production) and normalized per gram of carbon material in the cathode to facilitate the comparison of the different cathodes. The theoretical concentration of H_2O_2 corresponding to 100% current efficiency has also been indicated for clarity, as well as control data for the Toray paper support. It should be mentioned that the electric charge passing through the cells is different for each carbon, as this parameter depends on the current density recorded (i.e., electrolysis were carried out in potentiostatic mode).

With the exception of sample Gra, the carbons from Groups I and II exhibited the highest production of H_2O_2 (absolute and normalized values). This agrees with the pre-screening data from the LSV curves in a glassy carbon support (Fig. 2). The production of H_2O_2 matched the theoretical production for a 100 % of FE at low total charge values for both groups. At higher total charge values (corresponding to longer electrolysis times), the production rate stabilized reaching a plateau value. A decrease in the FE at long times was rather expected, likely due to the contribution of parasitic reactions in non-separated electrochemical cells, as the oxidation (r4) or the reduction (r5) of hydrogen peroxide [40, 58, 59].

$$H_2O_{2\,(aq)} \rightarrow 2H^+ + 2e^- + O_{2\,(g)} \qquad E^0 = 1.20\ (vs\ RHE) \qquad (r4)$$

$$H_2O_{2\,(aq)} + 2H^+_{(aq)} + 2e^- \rightarrow 2H_2O_{(aq)} \quad E^0 = 1.78\ (vs\ RHE) \qquad (r5)$$

These reactions are expected to increase with the concentration of hydrogen peroxide, and may be important since we have used a non-separated cell configuration in this study. They can be minimized in separated and flow-cells, thus increasing the production of hydrogen peroxide. Optimizing the hydrogen peroxide has not been considered in this study, which focuses on comparing the electrocatalytic performance of a pool of carbon cathodes.

With the exception of samples PCC and PCKOH (both obtained from the same precursor), carbons from Groups III and IV showed similar H_2O_2 production following overlapping profiles. This is interesting since these carbons showed different electrocatalytic activity in the pre-screening LSV curves in small dimension electrodes

(Fig. 2). Such differences are no longer observed when the electrochemical production of H_2O_2 is carried out in larger electrodes and for longer times.

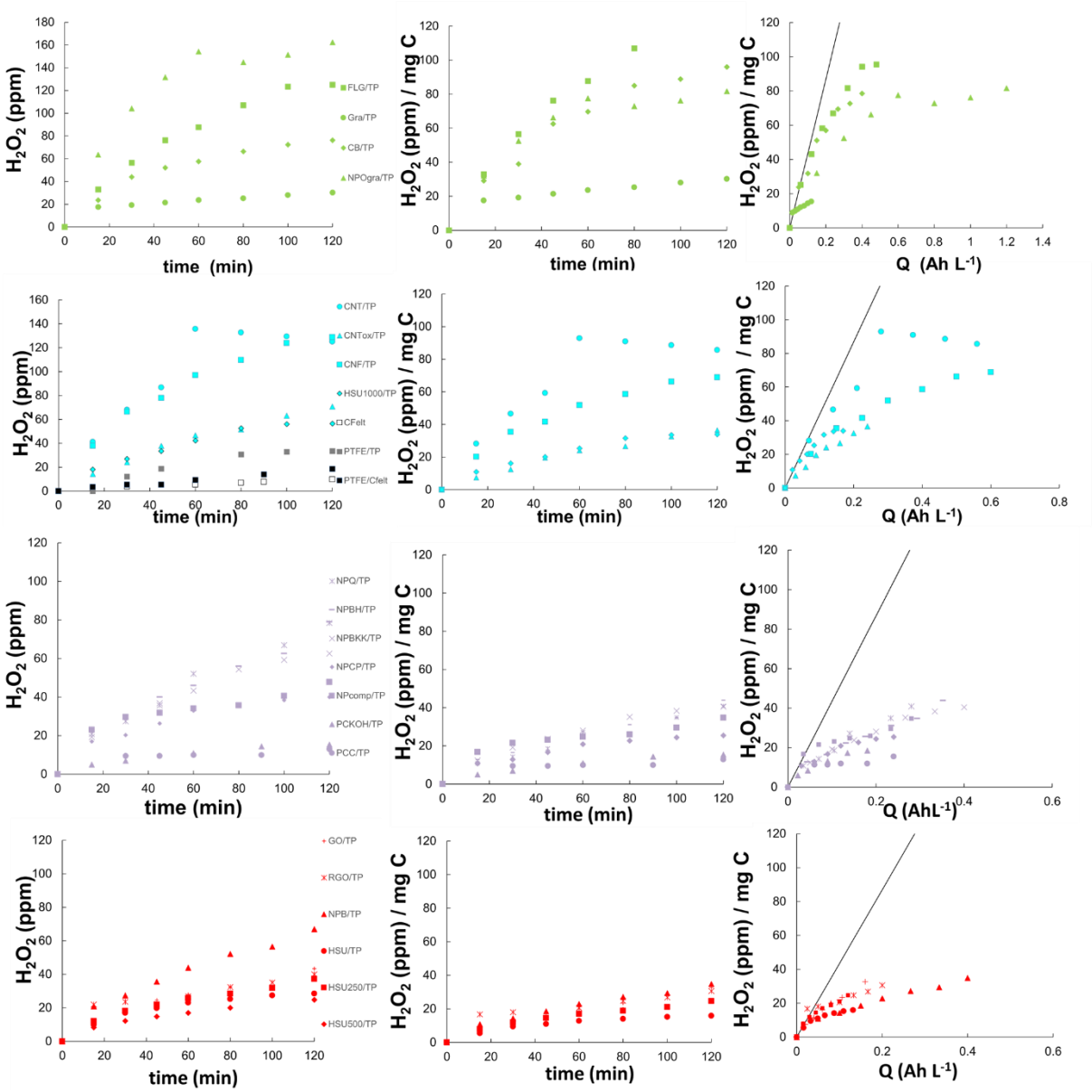

Figure 4. Production of H_2O_2 per mg of carbon material in the series of X/TP electrodes with the applied electric charge in potentiostatic mode (-0.9 V vs SCE) and in 0.05 M Na_2SO_4: a) group I; b) group II, c) group III; d) group IV. Line represents the theoretical amount of H_2O_2 for a 100% faradaic efficiency. Control assays corresponding to Toray Paper and Carbon Felt are included for comparison. Working electrode support: Toray paper; counter electrode: graphite rod; reference electrode: saturated calomel (SCE).

In this regard, the surface chemistry became a less important parameter in the electrocatalytic activity of the carbons in 4 cm^2 electrodes, as seen in the similar

production profiles of electrodes GO/TP and rGO/TP, as well as the series HSU/TP and its derivatives after thermal annealing at 250, 500 and 1000ºC. Hence, the electron transfer (i.e., electronic conductivity) would seem to be the parameter governing the overall performance in the large electrodes and at long electrolysis times.

Fig. 5 shows the dependence of the FE at an applied electric charge of 0.12 Ah L^{-1} of the electrochemical production of H_2O_2 for all the X/TP cathodes, and correlations with various physicochemical parameters of the carbons. The FE was calculated at the highest electric charge value where there is a linear increase with the concentration of H_2O_2 for all the carbons (for comparison purposes). Interestingly, the highest H_2O_2 production was obtained for carbons of Group I, whereas the FE was higher for the carbons of Group II (ca. 0.8 $^{o}/_{1}$ for CNF). To understand this behavior, it should be reminded that the FE is a concept related with the selectivity for reducing O_2 to generate H_2O_2. Thus, the high production in cathode NPQgra accompanied with a FE of ca. 0.52 $^{o}/_{1}$, indicates the existence of parallel reactions (typically HER or 4e-ORR) that compete with the electrochemical generation of hydrogen peroxide.

The porosity of the carbon materials does not seem to be a relevant parameter on the electrocatalytic activity, with random correlations in some groups between the surface area and/or microporosity of the carbons and the performance (Fig. 5b). This suggests that high micropore volumes associated to high surface areas that correspond to carbons of group III and IV are neither primary catalytic sites nor relevant gas transfer channels in the transport/diffusion of dissolved oxygen or the as-generated H_2O_2 [45, 57]. On the contrary, low values of specific surface area of carbons in group I and II show a better performance with faradaic efficiencies higher than 0.5 $^{o}/_{1}$.

For Groups I and II, the FE at a constant applied electric charge followed a rather linear increasing trend with the electrical conductivity; this was not the case for the other carbons (Fig. 5b,c). The electrical conductivity of the electrodes is related to the charge transfer processes occurring at the electrode interface. Thus, high conductivities are needed to increase the current response and minimize current losses. For Group IV, faradaic efficiencies ranged between 0.3-0.6 $^{o}/_{1}$, despite all the carbons display similar (very low) electrical conductivity. To explain the behavior of carbons in group IV, the differences in the structural features and/or composition of the carbons must be considered.

The correlation between the FE and some structural parameters of the carbons obtained from the analysis of Raman spectra is shown in Fig. 5c,e. Indeed, faradaic efficiencies

higher than 0.5 $^{o}/_{1}$ were obtained for those carbons displaying A_D/A_G ratios lower than 1.5 (mainly carbons from Groups I and II). According to literature, A_D/A_G values above 1.5 are characteristic of disordered carbons with small size aromatic domains associated to high density of structural defects (such as sp^3 hybridization, impurity atoms, vacancies, grain boundaries, loops...) [60]. The FE of the X/TP cathodes also followed a clear decreasing correlation with the width of the D band, as also discussed for the net current density (I_{net} O_2-He) determined in the screening LSV curves recorded with the X/GC electrodes (Fig. 3). In this line, Csp^3-bonds and structural defects have been reported as the active sites for the 2e-ORR to generate H_2O_2 [18]. These are considered active sites for favoring the adsorption of O_2, since oxygen interactions with carbon surfaces at room temperature are related to unsaturated carbon atoms on the carbon surface (i.e., structural defects and dangling bonds) [59].

Our data shows that structural defects in carbon-based cathodes play a pivotal role in their electrocatalytic activity for the $2e^-$ORR [61]. More specifically, an A_D/A_G threshold value of 1.5 could be used to discriminate the electrocatalytic activity of the carbon cathodes for the $2e^-$ORR, with high production rates (absolute production) and good faradaic efficiency (selectivity).

The performance of the carbon felt cathode (considered as a benchmark carbon cathode in many electrochemical applications) of similar dimensions was very poor in terms of FE and H_2O_2 production (Figs. 2 and 4). Despite the coating of the carbon felt with PTFE layer improved the electrocatalytic performance, it was still lower that most of the studied cathodes, particularly those from Group II where this material would be classified according to the composition, structure and conductivity (Fig. 1). We attribute this to the thickness of the carbon felt compared to the X/TP electrodes (ca. 12 vs 0.19 mm, respectively), that would affect the diffusion of oxygen through the electrode and would hinder a proper comparison of the performance.

Regarding functionalization, no significant differences were observed in the electrocatalytic activity of the series of hydrochars annealed at different temperatures, with similar FE of ca. 0.4 $^{o}/_{1}$ for the samples treated up to 500ºC. This is attributed to the fact that the structural parameters and conductivity of the carbons remained rather unchanged (e.g. A_D/A_G above the threshold of 1.5). In contrast, the FE increased for the sample treated at 1000ºC, which displayed lower structural defects (A_D/A_G of 1.5). Similarly, the FE of samples NPQ (Group III) and NPQgra (Group I) is similar (ca 0.5 $^{o}/_{1)}$, despite the A_{D1}/A_G ratio decreased from 2.1 to 1.2 after the graphitization. For

Group II (samples CNT and CNTox), the drop in FE should be linked to the slightly deterioration of the electrical conductivity upon oxidation, since the A_D/A_G ratio remained constant upon oxidation (Table S2).

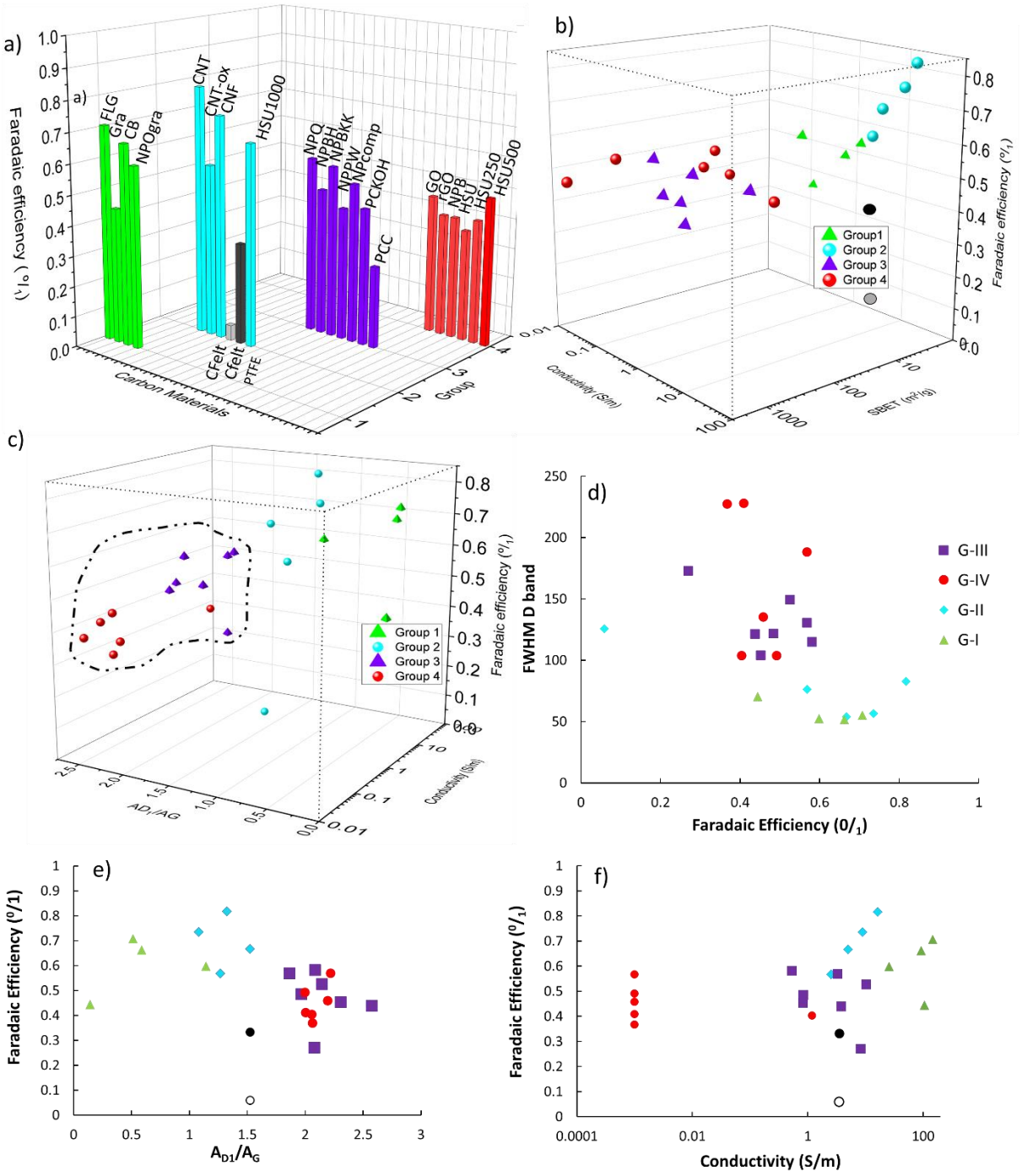

Fig. 5. (a) Faradaic efficiency of H_2O_2 production at an applied electric charge of 0.12 Ah L^{-1} using 4 cm^2 electrodes; (b) Faradaic efficiency of H_2O_2 production (Z axis) at an applied electric charge of 0.12 Ah L^{-1} with electrical conductivity (Y axis) and specific BET surface area (x axis); (c) Faradaic efficiency of H_2O_2 production (Z axis) vs A_D/A_G ratio (Y axis) and electrical conductivity (X axis); (d) Correlation between the FWMH of D band and the faradaic efficiency; (e) Correlation between the ratio A_{D1}/ A_G of

Raman spectra; (f) Correlation between electrical conductivity and faradaic efficiency. Working electrode: Toray Paper (4 cm^2); counter electrode: graphite rod; reference electrode: saturated calomel (SCE). Grey circle: Carbon Felt; black circle: Carbon Felt with PTFE).

3.4 Energy consumption of the cathodes

Fig. 6 shows the calculations of the energy consumption per gram of H_2O_2 for the different carbon cathodes, using two different criteria: (1) constant applied electric charge of 0.12 Ah L^{-1} (Fig. 6a) and (2) the production of 20 mg L^{-1} of H_2O_2 (Fig. 6b). These values of applied electric charge and H_2O_2 production were selected to be able to carry out the comparison of the 22 carbon materials studied in this work (given their large differences in electrocatalytic performance). Data of the benchmark carbon felt electrode in two electrode configurations (with and without a PTFE coating) is included for a fair comparison. Overall, the energy consumption of the carbon cathodes was rather low (especially for those carbons classified in Groups I and II), and in all the cases lower than that of the carbon felt benchmark. In this regard, it should be mentioned that the incorporation of a PTFE coating layer to the carbon felt significantly increased the FE and reduced the energy consumption, as previously stated in literature[55].

For an applied electric charge of 0.12 Ah L^{-1}, the energy consumption of all carbons is rather similar, despite FE span from 0.3 to 0.8 $^{o}/_{1}$. This is most likely due to the relatively low applied electric charge, that minimizes the decomposition of H_2O_2 (this being more important as the concentration of hydrogen peroxide increases, as discussed above) and that corresponds to short electrolysis times (Table S3). The balanced performance of samples from Groups III and IV in terms of electrochemical H_2O_2 production and energy consumption at short electrolysis times should be highlighted. Particularly if it is considered that many of these carbons are low cost materials that can be easily prepared from abundant and renewable precursors (including wastes), compared to carbons of Groups I and II. This represents an advantage to push their application in electrochemical processes and it would contribute to develop sustainable and cost-efficient electrochemical technologies based on circular economy processes involving materials' preparation.

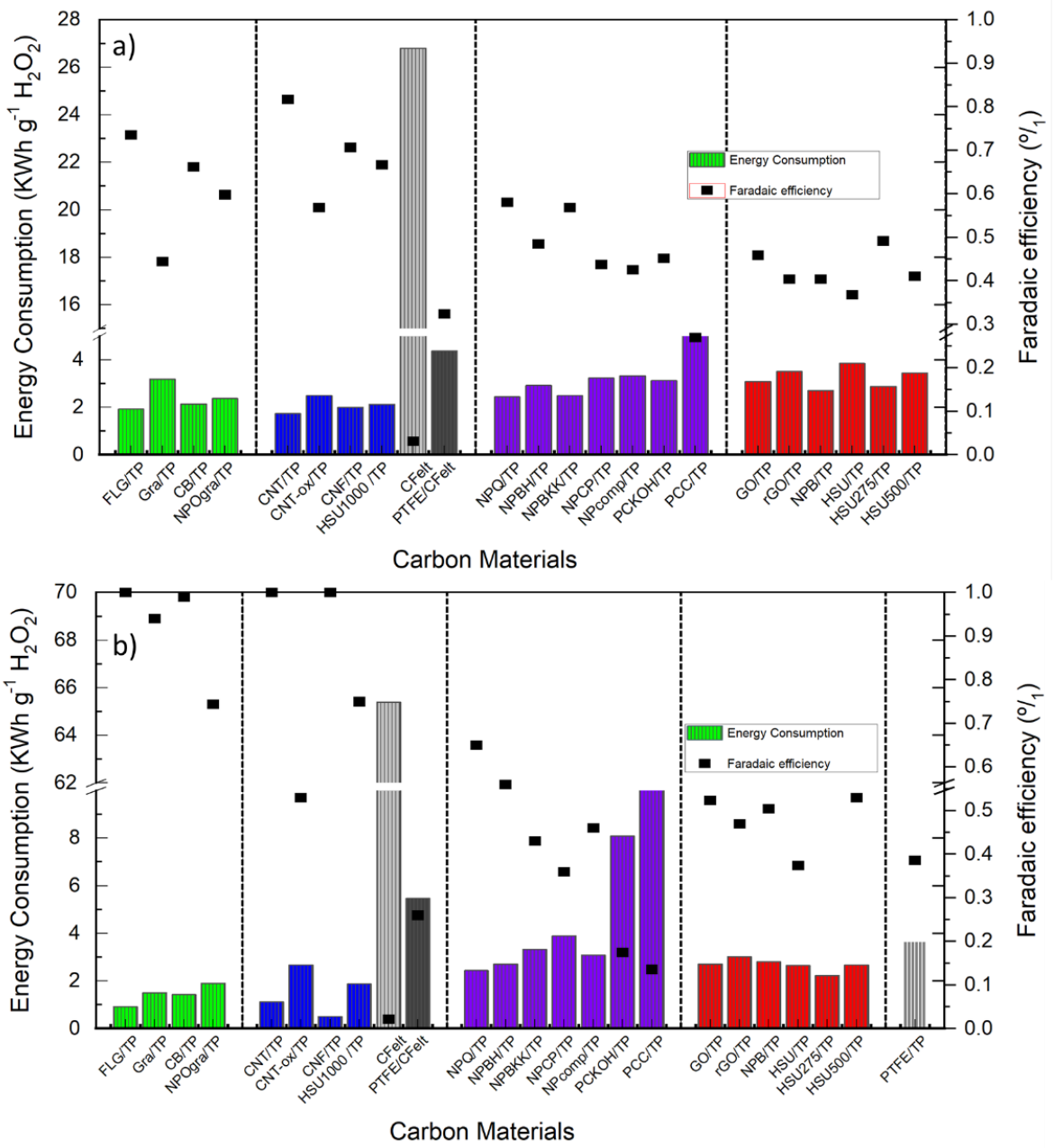

Fig. 6. Energy consumption and faradaic efficiency for the production of hydrogen peroxide calculated for the electrodes casted on TP (4 cm^2): (a) at an applied charge of 0.12 Ah L^{-1}; (b) for the production of 20 mg L^{-1} of H_2O_2. Values corresponding to carbon felt electrodes with and without PTFE coating have been added for comparison purposes.

On the other hand, when the energy consumption was expressed as the energy required to reach 20 mg L^{-1} H_2O_2, important differences were observed among the samples. Indeed, the energy consumption of carbons from Groups III and IV is significantly higher than that of Groups I and II, being the effect more pronounced for samples PCKOH/TP and PCC/TP (both obtained from the same precursor). This behavior is attributed to the longer times needed for carbons from Groups III and IV to produce

20 mg L^{-1} H_2O_2 (Fig. 4), whereas shorter times were involved for the calculations at an applied charge of 0.12 Ah L^{-1}. This points out that other factors may need to be considered for further optimizing the use of these carbons, such as using divided or flow cells to reduce side reactions that decompose H_2O_2 [58] or gas diffusion cathodes to reduce O_2 mass-transfer limitations [62]. Regarding Group II, the energy consumption of CNT-ox/TP is twice larger than that of CNT/TP, revealing the negative impact of the surface functionalization of the carbon cathode (structural parameters remained similar).

Conclusions

We have investigated the dependence of the electrocatalytic activity of carbon cathodes through 2e-ORR to produce hydrogen peroxide, with the characteristics of the carbon materials, by analyzing a pool of 22 carbons with varied physicochemical and structural properties. Electrocatalytic tests have been performed in small (0.2 cm^2) and large (4 cm^2) electrodes. Our data has shown that the electrocatalytic activity of carbon cathodes to produce hydrogen peroxide is a complex process that requires balanced characteristics in the electrodes to assure good electron transfer and O_2 mass transfer. While electrical conductivity of the carbons is important, the structural defects play a key role in their electrocatalytic activity, with less impact on composition and porosity. This dependence is more pronounced when the electrocatalytic tests are carried out in large electrodes and after various hours (ca. 150 minutes). In contrast, when the electrocatalytic tests are run in small electrodes (assays of 2-3 min, typically LSV data reported in the literature), the different performance due to chemical composition of the electrodes is no longer relevant in the overall production rate and faradaic efficiencies. Thus, it is of paramount importance to perform screening tests in large electrodes to validate the electrocatalytic performance of the cathodes for further process engineering.

Regarding the structure of the carbon materials, two parameters have been identified as reliable performance indicators to discriminate the electrocatalytic activity of the carbon cathodes. A_D/A_G ratio below 1.5 and a FWMH of the D band below 100 can be used as threshold values to identify carbon cathodes with potential electrocatalytic activity in terms of high production rates and selectivity towards the $2e^-$ORR. Both indicators are in agreement with the catalytic data obtained from the 0.2 and 4 cm^2 electrodes.

The highest H_2O_2 production yields of the analyzed carbons were obtained for carbon nanotubes and carbon nanofibers, outperforming common carbon benchmarks for this

application -i.e., carbon black, carbon felt-. Furthermore, a good catalytic activity was obtained with low-cost and disordered carbon cathodes with moderate electrical conductivity and density of structural defects, both in terms of overall production rate, selectivity and energy consumption.

Acknowledgements

M.Muñoz-Morales and J.Llanos wish to express their gratitude to *Junta de Comunidades de Castilla-La Mancha, Diputación de Albacete* and UCLM for the funding (grants SBPLY/21/180501/000058 and DIPUAB-2022 MUÑOZMORALES respectively). Conchi Ania thanks the funding from the European Union's Horizon 2020 research and innovation program (grant agreement 776816) and Region Centre Val de Loire (PRESERVE, grant EX010666). The authors acknowledge Dr. Vautrin-Ul and Mme. Jebali from ICMN (Orléans) for the access to contact angle and RRDE measurements.

Declaration of competing interest

The authors declare that they have no known competing financial interests or personal relationships that could have appeared to influence the work reported in this paper.

Appendix A. Supplementary data

Supplementary data to this article is available at .....

References

[1] J. Vidal, C. Saez, P. Cañizares, V. Navarro, R. Salazar, M.A. Rodrigo, ZVI – Reactive barriers for the remediation of soils polluted with clopyralid: Are they really Worth?, Chemical Engineering Journal 350 (2018) 100-107.
[2] Y. Yang, Y. Xue, H. Zhang, H. Chang, Flexible H2O2 microfluidic fuel cell using graphene/Prussian blue catalyst for high performance, Chemical Engineering Journal 369 (2019) 813-817.
[3] M.H. Tran, B.J. Park, B.H. Kim, H.H. Yoon, Mesoporous silica template-derived nickel-cobalt bimetallic catalyst for urea oxidation and its application in a direct urea/H2O2 fuel cell, Int. J. Hydrogen Energy 45(3) (2020) 1784-1792.
[4] HYDROGEN PEROXIDE MARKET - GROWTH, TRENDS, COVID-19 IMPACT, AND FORECASTS (2022 - 2027). https://www.mordorintelligence.com/industry-reports/hydrogen-peroxide-market.
[5] J.M. Campos-Martín, G. Blanco-Brieva, J.L.G. Fierro, Hydrogen peroxide synthesis: an outlook beyond the anthraquinone process, Angewandte Chemie 45 42 (2006) 6962-84.

[6] S. Yang, A. Verdaguer-Casadevall, L. Arnarson, L. Silvioli, V. Čolić, R. Frydendal, J. Rossmeisl, I. Chorkendorff, I.E.L. Stephens, Toward the Decentralized Electrochemical Production of H2O2: A Focus on the Catalysis, ACS Catalysis 8(5) (2018) 4064-4081.
[7] R.G. Hans-Joaquin, P, Production of Hydrogen Peroxide U.S. Patent, 1940.
[8] F.F. Rust, Manufacture of Hydrogen Peroxide, United States Patent, U.S., 1959.
[9] J.M. Campos-Martin, G. Blanco-Brieva, J.L.G. Fierro, Hydrogen Peroxide Synthesis: An Outlook beyond the Anthraquinone Process, Angew. Chem. Int. Ed. 45(42) (2006) 6962-6984.
[10] E. Petrucci, A. Da Pozzo, L. Di Palma, On the ability to electrogenerate hydrogen peroxide and to regenerate ferrous ions of three selected carbon-based cathodes for electro-Fenton processes, Chemical Engineering Journal 283 (2016) 750-758.
[11] D. Song, J. Li, Z. Wang, C. Zhao, Performance of graphite felt as anodes in the electro-Fenton oxidation systems: Changes in catalysis, conductivity and adsorption properties, Appl. Surf. Sci. 532 (2020) 147450.
[12] A. Özcan, Y. Şahin, A. Savaş Koparal, M.A. Oturan, Carbon sponge as a new cathode material for the electro-Fenton process: Comparison with carbon felt cathode and application to degradation of synthetic dye basic blue 3 in aqueous medium, Journal of Electroanalytical Chemistry 616(1) (2008) 71-78.
[13] B. Ramírez-Pereda, A. Álvarez-Gallegos, J.G. Rangel-Peraza, Y.A. Bustos-Terrones, Kinetics of Acid Orange 7 oxidation by using carbon fiber and reticulated vitreous carbon in an electro-Fenton process, Journal of Environmental Management 213 (2018) 279-287.
[14] J.D. García-Espinoza, I. Robles, A. Durán-Moreno, L.A. Godínez, Study of simultaneous electro-Fenton and adsorption processes in a reactor containing porous carbon electrodes and particulate activated carbon, Journal of Electroanalytical Chemistry 895 (2021) 115476.
[15] H.H. Phan Quang, T.P. Nguyen, D.D. Duc Nguyen, L.T. Ngoc Bao, D.C. Nguyen, V.-H. Nguyen, Advanced electro-Fenton degradation of a mixture of pharmaceutical and steel industrial wastewater by pallet-activated-carbon using three-dimensional electrode reactor, Chemosphere 297 (2022) 134074.
[16] P. Dong, X. Chen, M. Guo, Z. Wu, H. Wang, F. Lin, J. Zhang, S. Wang, C. Zhao, H. Sun, Heterogeneous electro-Fenton catalysis with self-supporting CFP@MnO2-Fe3O4/C cathode for shale gas fracturing flowback wastewater, Journal of Hazardous Materials 412 (2021) 125208.
[17] G.d.O.S. Santos, K.I.B. Eguiluz, G.R. Salazar-Banda, C. Saez, M.A. Rodrigo, Testing the role of electrode materials on the electro-Fenton and photoelectro-Fenton degradation of clopyralid, Journal of Electroanalytical Chemistry 871 (2020) 114291.
[18] K. Wang, J. Huang, H. Chen, Y. Wang, S. Song, Recent advances in electrochemical 2e oxygen reduction reaction for on-site hydrogen peroxide production and beyond, Chem Commun (Camb) 56(81) (2020) 12109-12121.
[19] H.W. Kim, M.B. Ross, N. Kornienko, L. Zhang, J. Guo, P. Yang, B.D. McCloskey, Efficient hydrogen peroxide generation using reduced graphene oxide-based oxygen reduction electrocatalysts, Nature Catalysis 1(4) (2018) 282-290.
[20] W. Zhou, L. Xie, J. Gao, R. Nazari, H. Zhao, X. Meng, F. Sun, G. Zhao, J. Ma, Selective H2O2 electrosynthesis by O-doped and transition-metal-O-doped carbon cathodes via O2 electroreduction: A critical review, Chemical Engineering Journal 410 (2021) 128368.
[21] J. An, N. Li, Q. Zhao, Y. Qiao, S. Wang, C. Liao, L. Zhou, T. Li, X. Wang, Y. Feng, Highly efficient electro-generation of H2O2 by adjusting liquid-gas-solid three phase interfaces of porous carbonaceous cathode during oxygen reduction reaction, Water Research 164 (2019) 114933-114933.
[22] H. Zhang, Y. Li, Y. Zhao, G. Li, F. Zhang, Carbon Black Oxidized by Air Calcination for Enhanced H2O2 Generation and Effective Organics Degradation, ACS Applied Materials & Interfaces 11(31) (2019) 27846-27853.
[23] J.F. Pérez, S. Sabatino, A. Galia, M.A. Rodrigo, J. Llanos, C. Sáez, O. Scialdone, Effect of air pressure on the electro-Fenton process at carbon felt electrodes, Electrochim. Acta 273 (2018) 447-453.

[24] T.X.H. Le, T.V. Nguyen, Z. Amadou Yacouba, L. Zoungrana, F. Avril, D.L. Nguyen, E. Petit, J. Mendret, V. Bonniol, M. Bechelany, S. Lacour, G. Lesage, M. Cretin, Correlation between degradation pathway and toxicity of acetaminophen and its by-products by using the electro-Fenton process in aqueous media, Chemosphere 172 (2017) 1-9.
[25] V. Poza-Nogueiras, Á. Moratalla, M. Pazos, Á. Sanromán, C. Sáez, M.A. Rodrigo, Towards a more realistic heterogeneous electro-Fenton, Journal of Electroanalytical Chemistry 895 (2021) 115475.
[26] V. Poza-Nogueiras, Á. Moratalla, M. Pazos, Á. Sanromán, C. Sáez, M.A. Rodrigo, Exploring the pressurized heterogeneous electro-Fenton process and modelling the system, Chemical Engineering Journal 431 (2022) 133280.
[27] G. Ren, M. Zhou, M. Liu, L. Ma, H. Yang, A novel vertical-flow electro-Fenton reactor for organic wastewater treatment, Chemical Engineering Journal 298 (2016) 55-67.
[28] Y.Y. Chu, Y. Qian, W.J. Wang, X.L. Deng, A dual-cathode electro-Fenton oxidation coupled with anodic oxidation system used for 4-nitrophenol degradation, Journal of Hazardous Materials 199-200 (2012) 179-185.
[29] P.J.M. Cordeiro-Junior, M.S. Kronka, L.A. Goulart, N.C. Veríssimo, L.H. Mascaro, M.C.d. Santos, R. Bertazzoli, M.R.d.V. Lanza, Catalysis of oxygen reduction reaction for H2O2 electrogeneration: The impact of different conductive carbon matrices and their physicochemical properties, Journal of Catalysis 392 (2020) 56-68.
[30] M.H.M.T. Assumpção, R.F.B. De Souza, D.C. Rascio, J.C.M. Silva, M.L. Calegaro, I. Gaubeur, T.R.L.C. Paixão, P. Hammer, M.R.V. Lanza, M.C. Santos, A comparative study of the electrogeneration of hydrogen peroxide using Vulcan and Printex carbon supports, Carbon 49(8) (2011) 2842-2851.
[31] C. Li, C. Hu, Y. Song, Y.-M. Sun, W. Yang, M. Ma, Graphene-based synthetic fabric cathodes with specific active oxygen functional groups for efficient hydrogen peroxide generation and homogeneous electro-Fenton processes, Carbon 186 (2022) 699-710.
[32] O.M. Cornejo, I. Sirés, J.L. Nava, Cathodic generation of hydrogen peroxide sustained by electrolytic O2 in a rotating cylinder electrode (RCE) reactor, Electrochim. Acta 404 (2022) 139621.
[33] E. Jung, H. Shin, W. Hooch Antink, Y.-E. Sung, T. Hyeon, Recent Advances in Electrochemical Oxygen Reduction to H2O2: Catalyst and Cell Design, ACS Energy Letters 5(6) (2020) 1881-1892.
[34] J. Zhang, G. Zhang, S. Jin, Y. Zhou, Q. Ji, H. Lan, H. Liu, J. Qu, Graphitic N in nitrogen-Doped carbon promotes hydrogen peroxide synthesis from electrocatalytic oxygen reduction, Carbon 163 (2020) 154-161.
[35] K.M. Nair, V. Kumaravel, S.C. Pillai, Carbonaceous cathode materials for electro-Fenton technology: Mechanism, kinetics, recent advances, opportunities and challenges, Chemosphere 269 (2021) 129325.
[36] R.B. Moreira FC , Enric Brillas, Vítor J.P. Vilar, Electrochemical advanced oxidation processes: A review on their application to synthetic and real wastewaters, Applied Catalysis B: Environmental 202 (2017) 217-261.
[37] C. Li, C. Hu, Y. Song, Y.M. Sun, W. Yang, M. Ma, Graphene-based synthetic fabric cathodes with specific active oxygen functional groups for efficient hydrogen peroxide generation and homogeneous electro-Fenton processes, Carbon 186 (2022) 699-710.
[38] S. Zhang, S. Li, J. Liu, L. Kan, F. Rong, L. He, Z. Zhang, Multiple active cobalt species embedded in microporous nitrogen-doped carbon network for the selective production of hydrogen peroxide, J. Colloid Interface Sci. 631 (2023) 101-113.
[39] T. Murayama, I. Yamanaka, Electrosynthesis of Neutral H2O2 Solution from O2 and Water at a Mixed Carbon Cathode Using an Exposed Solid-Polymer-Electrolyte Electrolysis Cell, The Journal of Physical Chemistry C 115 (2011).
[40] P. Ma, H. Ma, A. Galia, S. Sabatino, O. Scialdone, Reduction of oxygen to H2O2 at carbon felt cathode in undivided cells. Effect of the ratio between the anode and the cathode surfaces

and of other operative parameters, Separation and Purification Technology 208 (2019) 116-122.
[41] A. Casanova, R. Rincón, J. Muñoz, C.O. Ania, M.D. Calzada, Optimizing high-quality graphene nanoflakes production through organic (bio)-precursor plasma decomposition, Fuel Process. Technol. 212 (2021) 106630.
[42] L.F. Velasco, I.M. Fonseca, J.B. Parra, J.C. Lima, C.O. Ania, Photochemical behaviour of activated carbons under UV irradiation, Carbon, 2012, pp. 249-258.
[43] L.F. Velasco, C.O. Ania, Understanding phenol adsorption mechanisms on activated carbons, Adsorption 17(1) (2011) 247-254.
[44] J.B. Parra, C.O. Ania, A. Arenillas, J.J. Pis, Textural characterisation of activated carbons obtained from poly(ethylene terephthalate) by carbon dioxide activation, 2002.
[45] A. Casanova, A. Gomis-Berenguer, A. Canizares, P. Simon, D. Calzada, C.O. Ania, Carbon black as conductive additive and structural director of porous carbon gels, Materials 13(1) (2020).
[46] L.F. Velasco, M. Haro, J. Parmentier, R. Gadiou, C. Vix-Guterl, C.O. Ania, Tuning the Photocatalytic Activity and Optical Properties of Mesoporous TiO₂ Spheres by a Carbon Scaffold, Journal of Catalysts 2013 (2013) 178512.
[47] F. Yu, M. Zhou, X. Yu, Cost-effective electro-Fenton using modified graphite felt that dramatically enhanced on H2O2 electro-generation without external aeration, Electrochim. Acta 163 (2015) 182-189.
[48] J.F. Pérez, A. Galia, M.A. Rodrigo, J. Llanos, S. Sabatino, C. Sáez, B. Schiavo, O. Scialdone, Effect of pressure on the electrochemical generation of hydrogen peroxide in undivided cells on carbon felt electrodes, Electrochim. Acta 248 (2017) 169-177.
[49] M. Panizza, G. Cerisola, Direct And Mediated Anodic Oxidation of Organic Pollutants, Chemical Reviews 109 (2009) 6541-6569.
[50] E. Brillas, I. Sirés, M.A. Oturan, Electro-Fenton Process and Related Electrochemical Technologies Based on Fenton's Reaction Chemistry, Chemical Reviews 109(12) (2009) 6570-6631.
[51] A.K. Jain, M.N. Murty, P.J. Flynn, Data clustering: a review, ACM Comput. Surv. 31 (1999) 264-323.
[52] S.C. Johnson, Hierarchical clustering schemes, Psychometrika 32 (1967) 241-254.
[53] Z. Zhou, Z. Pei, L. Wei, S. Zhao, X. Jian, Y. Chen, Electrocatalytic hydrogen evolution under neutral pH conditions: current understandings, recent advances, and future prospects, Energy & Environmental Science 13(10) (2020) 3185-3206.
[54] Q. Zhao, J. An, S. Wang, Y. Qiao, C. Liao, C. Wang, X. Wang, N. Li, Superhydrophobic Air-Breathing Cathode for Efficient Hydrogen Peroxide Generation through Two-Electron Pathway Oxygen Reduction Reaction, ACS Applied Materials & Interfaces 11(38) (2019) 35410-35419.
[55] J.F. Pérez, C. Sáez, J. Llanos, P. Cañizares, C. López, M.A. Rodrigo, Improving the Efficiency of Carbon Cloth for the Electrogeneration of H2O2: Role of Polytetrafluoroethylene and Carbon Black Loading, Industrial & Engineering Chemistry Research 56(44) (2017) 12588-12595.
[56] A. Sadezky, H. Muckenhuber, H. Grothe, R. Niessner, U. Pöschl, Raman microspectroscopy of soot and related carbonaceous materials: Spectral analysis and structural information, Carbon 43(8) (2005) 1731-1742.
[57] O. Beyssac, B. Goffé, C. Chopin, J.N. Rouzaud, Raman spectra of carbonaceous material in metasediments: A new geothermometer, Journal of Metamorphic Geology - J METAMORPH GEOL 20 (2002) 859-871.
[58] T. Pérez, G. Coria, I. Sirés, J.L. Nava, A.R. Uribe, Electrosynthesis of hydrogen peroxide in a filter-press flow cell using graphite felt as air-diffusion cathode, Journal of Electroanalytical Chemistry 812 (2018) 54-58.

[59] J.F. Pérez, J. Llanos, C. Sáez, C. López, P. Cañizares, M.A. Rodrigo, Electrochemical jet-cell for the in-situ generation of hydrogen peroxide, Electrochemistry Communications 71 (2016) 65-68.
[60] P. Puech, M. Kandara, G. Paredes, L. Moulin, E. Weiss-Hortala, A. Kundu, N. Ratel-Ramond, J.-M. Plewa, R. Pellenq, M. Monthioux, Analyzing the Raman Spectra of Graphenic Carbon Materials from Kerogens to Nanotubes: What Type of Information Can Be Extracted from Defect Bands?, C 5(4) (2019) 69.
[61] R. Ma, G. Lin, Y. Zhou, Q. Liu, T. Zhang, G. Shan, M. Yang, J. Wang, A review of oxygen reduction mechanisms for metal-free carbon-based electrocatalysts, npj Computational Materials 5(1) (2019).
[62] J. Liao, S. Xie, J. Yao, D. Xu, P. Liao, Efficient hydrogen peroxide production at high current density by air diffusion cathode based on pristine carbon black, Journal of Electroanalytical Chemistry 904 (2022) 115938.

Appendix A. Supplementary data

Evaluating key properties of carbon materials as cathodes for the electro-generation of hydrogen peroxide

M. Muñoz-Morales[1,2] *, A. Ramírez[2], Aurelien Cañizares[1], J. Llanos[2], Conchi Ania[1]*

[1] CEMHTI, CNRS (UPR 3079), Université d'Orléans, 45071 Orléans, France.

[2] Chem. Eng. Dept., Faculty of Chemical Sciences & Technologies, Univ. Castilla La Mancha, Campus Universitario s/n 13071 Ciudad Real, Spain.

* corresponding authors: martin.munoz@uclm.es; conchi.ania@cnrs-orleans.fr

Supplementary File

Characterization techniques

The porosity of the materials was evaluated by N_2 adsorption isotherms at -196 °C in automatic volumetric analyzer from Micromeritics. The samples were initially degassed under vacuum at 120 °C for 17 h. The nitrogen adsorption isotherms were used to calculate the specific surface area (S_{BET}) and micropore volume using the Dubinin-Radushkevich equation [1]. Each isotherm was recorded in duplicate on fresh sample aliquots (error was below 2 %).

Elemental analysis of samples dried at 100 °C was measured in a LECO CHNS-932 (C, H, N, S) and a LECO-VTF-900 (O) analyzers.

Raman spectra were recorded in ambient conditions in a Renishaw InVia Qontor spectrometer equipped with 514.5 nm laser. The spectra were collected under a Leica DM2500 optical microscope with a x50 long working distance objective (ca. 10 mm). The scattered Raman light was dispersed by a holographic grating of 600 grooves/mm, in order to acquire the whole range of interest for carbons (500-5000 cm^{-1}). Each spectrum was recorded with an integration time of 5 s; data presented represents the average of three measurements. Deconvolution of Raman spectra was carried out by a fitting procedure using a linear baseline and Gaussian/Lorentzian functions, and the assignment of the peaks according to the ligature [2].

The electrical conductivity of the samples was measured using a four-point probe method following the general principles of ASTM standard methods D4496-87 [3]. Briefly, disk-shaped pellets of the samples (ca. 90 wt.% of carbon powders, 10 wt.% polyvinylidene fluoride binder) were prepared by compaction of the powders under 5 tons pressure. The diameter of the pellets was ca. 10 mm and their thickness varied between 0.10-0.16 mm (total weights between 8-12 mg). The resistance of the pellets was measured at room temperature and atmospheric pressure using a Keithley 2400 multimeter coupled with a 4 probes Everbeing SR-4 module to make the electrical contact, using the van der Pauw technique. It was followed the general principles of ASTM standard methods D4496-87 [4]. Briefly, a constant current (between 1-10 mA) was applied to the surface of the pellets through the probes, and the voltage drop was

recorded. The bulk resistivity of the samples (ρ), reciprocal of conductivity (σ) was calculated according to

$$\rho = \frac{V}{I}\frac{\pi}{\ln 2}t, \quad (1)$$

where *V* is the voltage drop (V), *I* is the current intensity (A), and *t* is the thickness of the pellets (m).

Linear sweep voltammetry (LSV) at a rotating ring-disk electrode (RRDE-3A, ALS, Japan) containing a 3 mm diameter glassy carbon disk surrounded by a Pt ring, in O_2-saturated 0.050 M Na_2SO_4 electrolyte using a VMP potentiostat. The measurements were made in a three-electrode cell that included the RRDE as working electrode, a graphite rod as counter electrode and an Ag/AgCl reference electrode, at a scan rate of 5 mV/s and rotation speeds (ω) between 500-5000 rpm. 20 μL of the inks of the carbon materials (10 mg/mL of carbon powders in 2-methyl propanol and 5 wt.% nafion) were drop-casted on the glassy carbon disk (loading 0.4 mg/cm^2). The number of electrons transferred during ORR (n) and the H_2O_2 yield were determined from the measured disk and ring currents (i_D and i_R, respectively), considering a collection efficiency (N) of 0.45 and according to the following equations:

$$\textbf{n electrons} = 4i_D/(i_D+i_R/N)$$

$$\textbf{H}_2\textbf{O}_2\textbf{ yield} = 100 * 2i_R/(Ni_D+i_R)$$

Contact angles θ (°) were measured to determine the hydrophilic and hydrophobic properties of materials and the electrodes (and investigate their wetting behavior). Measurements were performed based on the sessile drop method, using 2 μl drops of deionised water deposited on the samples with a micropipette in a Digitrop (GBX) instrument. The contact angle was measured after stabilization of the water droplet in contact with the material surface. Averages of three independent measurements were registered for each sample.

References

[1] Rouquerol, J.; Rouquerol, F.; Sing, K.S.W.; Llewellyn, P.; Maurin, G. *Adsorption by powders and porous solids: Principles, methodology and applications*, 2nd ed.; Academic Press: Oxford, UK, 2014.

[2] Sadezky, H. Muckenhuber, H. Grothe, R. Niessner, U. Pöschl, Raman microspectroscopy of soot and related carbonaceous materials: Spectral analysis and structural information, Carbon, 43 (2005) 1731-1742.

[3] ASTM D4496, Standard Test Method for D-C Resistance or Conductance of Moderately Conductive Materials Edition, May 1, 2013.

[4] Van der Pauw, L.J. A method of measuring specific resistivity and Hall effect of discs of arbitrary shapes. *Philips Res Repts* **1958**, *13*, 1-9.

List of Tables and Figures

Table S1. Elemental analysis (wt.% dry ash basis), electric conductivity and selected textural parameters of the studied carbon-based materials.

Groups	Carbon Material	C	H	N	O	S	Conductivity (S/m)	S_{BET} (m^2/g)	Vmicropores (cm^3/g)
I	FLG	99.8	0.1	0.0	0.1	0.001	146.7	255	0.077
I	Gra	99.8	0.1	0.0	0.1	0.1	104.8	9	0.002
I	CB	99.8	0.1	0.0	0.1	0.0	92.1	43	0.017
I	NPQgra	99.7	0.01	0.26	0.02	0	25.8	25	0.006
II	CNT	98.4	1.3	0.0	0.3	0.0	16.2	292	0.068
II	CNT-ox	92.3	2.5	0.0	5.2	0.0	2.56	284	0.106
II	CNF	96.8	1.6	0.3	1.3	0.0	8.9	154	0.057
II	HSU1000	94.6	2.1	0.1	3.1	0.1	4.97	393	0.155
II	CFelt	95.6	1.6	--	2.8	--	3.5	33	0.007
III	NPQ	96.6	0.6	0.7	2.1	0.0	0.53	1033	0.316
III	NPBH	93.1	0.9	0.1	6.0	0.0	0.85	1040	0.272
III	NPBKK	94.0	0.3	0.8	4.7	0.2	3.33	961	0.292
III	NPPW	99.2	0.3	0.0	0.6	0.0	3.80	1357	0.453
III	NPcomp	97.8	0.8	0.0	1.4	0.0	10.43	330	0.112
III	PCKOH	95.0	0.6	0.9	3.3	0.1	0.84	577	0.228
III	PCC	94.5	1.1	2.8	0.7	0.9	8.33	2	0.001
IV	GO	51.6	4.2	2.6	40.3	--	b.d.l.	9	0.001
IV	rGO	85.3	1.3	1.1	12.2	--	1.2	29	0.007
IV	NPB	84.7	2.6	0.1	12.7	0.0	0.005	1280	0.314
IV	HSU	70.5	4.6	0.1	24.8	0.1	b.d.l.	5	0.002
IV	HSU250	77.7	3.6	0.1	18.6	0.1	b.d.l.	16	0.004
IV	HSU500	85.5	3.1	0.1	11.2	0.1	b.d.l.	354	0.131

b.d.l. below detection limits

Table S2. Selected structural parameters of the studied carbon materials obtained from the deconvolution of the Raman spectra.

Groups	Carbon Material	A_{D1}	A_G	A_{D1}/A_G
I	FLG	30.50	59.28	0.51
I	Gra	11.90	84.05	0.19
I	CB	33.55	57.20	0.59
I	NPQgra	45.17	37.76	1.20
II	CNT	45.83	38.17	1.20
II	CNT-ox	46.45	37.79	1.23
II	CNF	44.81	41.45	1.08
II	HSU1000	51.33	33.69	1.52
II	CFelt	52.70	34.60	1.52
III	NPQ	29.23	28.37	2.09
III	NPBH	44.97	22.85	1.97
III	NPBKK	47.16	25.27	1.87
III	NPPW	60.52	23.50	2.58
III	NPcomp	43.49	20.25	2.15
III	PCKOH	53.775	23.27	2.31
III	PCC	50.45	23.93	2.11
IV	GO	52.27	23.80	2.20
IV	rGO	53.01	27.20	1.95
IV	NPB	49.41	22.26	2.22
IV	HSU	50.52	25.20	2.01
IV	HSU250	55.38	27.87	1.99
IV	HSU500	48.61	23.53	2.07

Table S3. Electrochemical parameters during H_2O_2 production using a 2 x 2 cm^2 Toray paper (TP) support and catalytic inks of the different carbon materials in a PTFE dispersion (ratio 1:30 wt.%). Counter Electrode: graphite rod; Reference electrode SCE; 0.05 M Na_2SO_4 electrolyte. Potentiostatic mode. Applied electric charge 0.12 A h L^{-1}.

Groups	Carbon Material	Intensity (A)	time (h)	[H_2O_2] (mg/L)	Faradaic Efficiency (%)
	Bare TP	0.0036	1.67	5.5	7.2
I	**FLG/TP**	0.012	0.5	56	73.6
I	**Gra/TP**	0.0029	2.01	33.8	44.4
I	**CB/TP**	0.01	0.60	50.4	66.2
I	**NPQgra/TP**	0.03	0.20	45.5	59.8
II	**CNT/TP**	0.014	0.43	62.2	81.7
II	**CNT-ox/TP**	0.006	1.00	43.3	56.9
II	**CNF/TP**	0.01	0.6	53.8	70.7
II	**HSU1000/TP**	0.005	1.00	42.3	66.7
II	**CFelt**	0.02	0.3	3.8	5.3
II	**CFelt (PTFE coated)**	0.018	0.15	11.2	32.7
III	**NPQ/TP**	0.007	0.86	44.2	58.1
III	**NPBH/TP**	0.0088	0.57	30.7	48.5
III	**NPBKK/TP**	0.01	0.60	43.3	56.9
III	**NPPW/TP**	0.006	1.00	33.3	43.8
III	**NPcomp/TP**	0.007	0.86	32.4	42.6
III	**PCKOH/TP**	0.045	1.33	15.4	43.3
III	**PCC/TP**	0.045	1.33	23.0	27.0
IV	**GO/TP**	0.004	1.50	34.9	45.9
IV	**rGO/TP**	0.005	1.20	30.8	40.4
IV	**NPB/TP**	0.007	0.60	44.0	56.8
IV	**HSU/TP**	0.0033	1.80	0.028	36.8
IV	**HSU250/TP**	0.003	2.00	37.4	49.2
IV	**HSU500/TP**	0.003	2.00	31.3	41.1

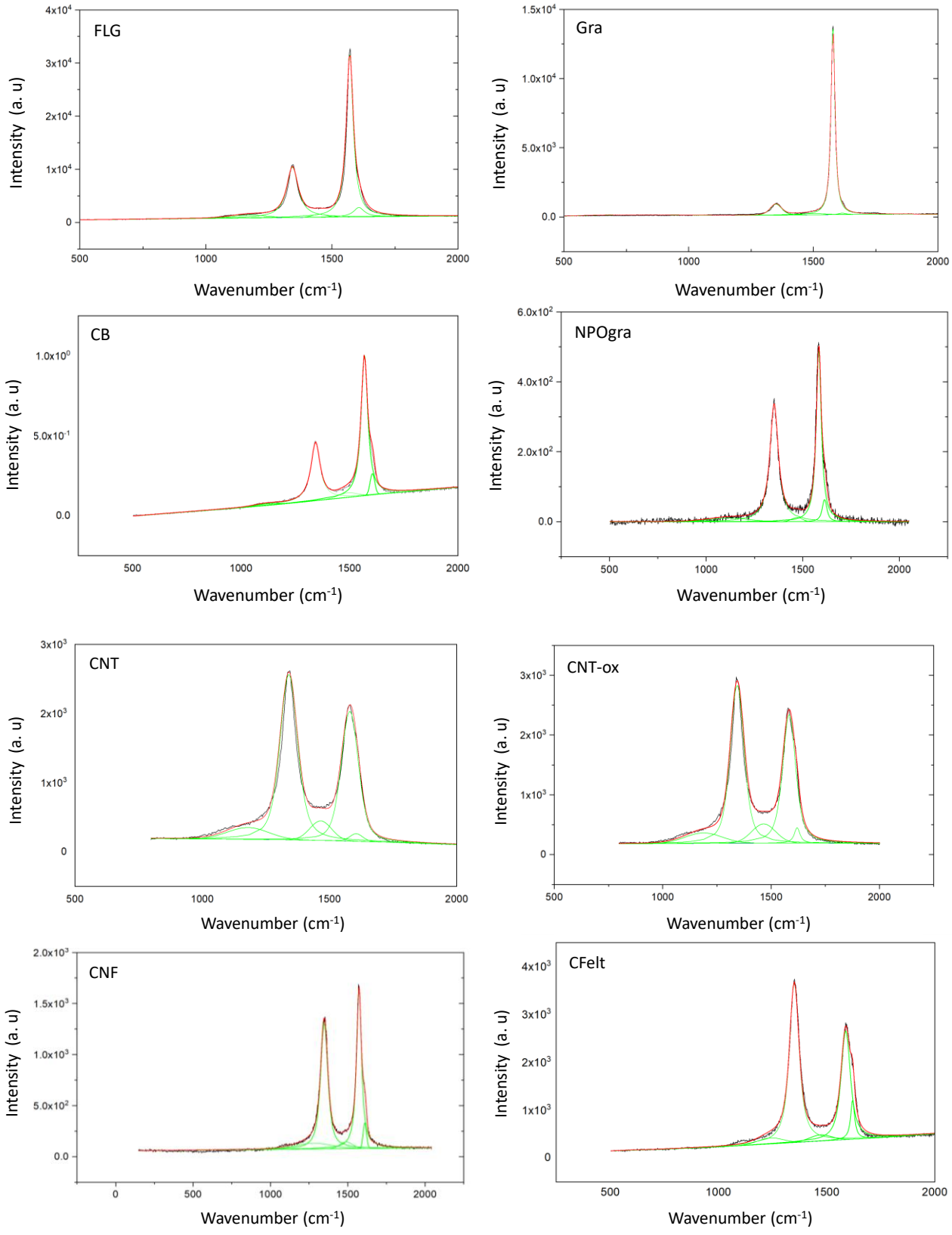

Figure S1. Raman spectra and deconvolution signals of the studied carbon materials. Spectra have deconvoluted according to Sadezky's 5-band model [2].

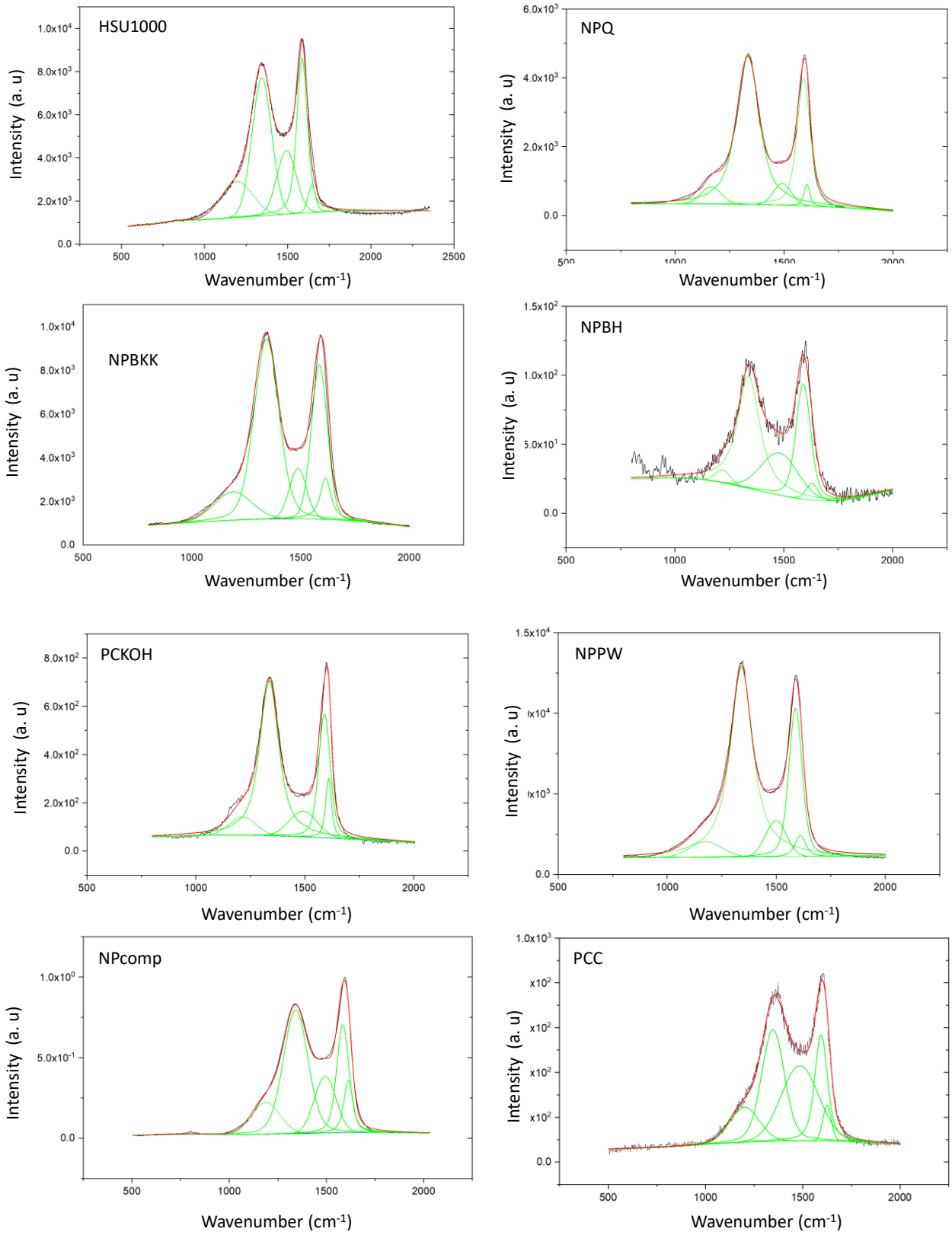

Figure S1. (continued)

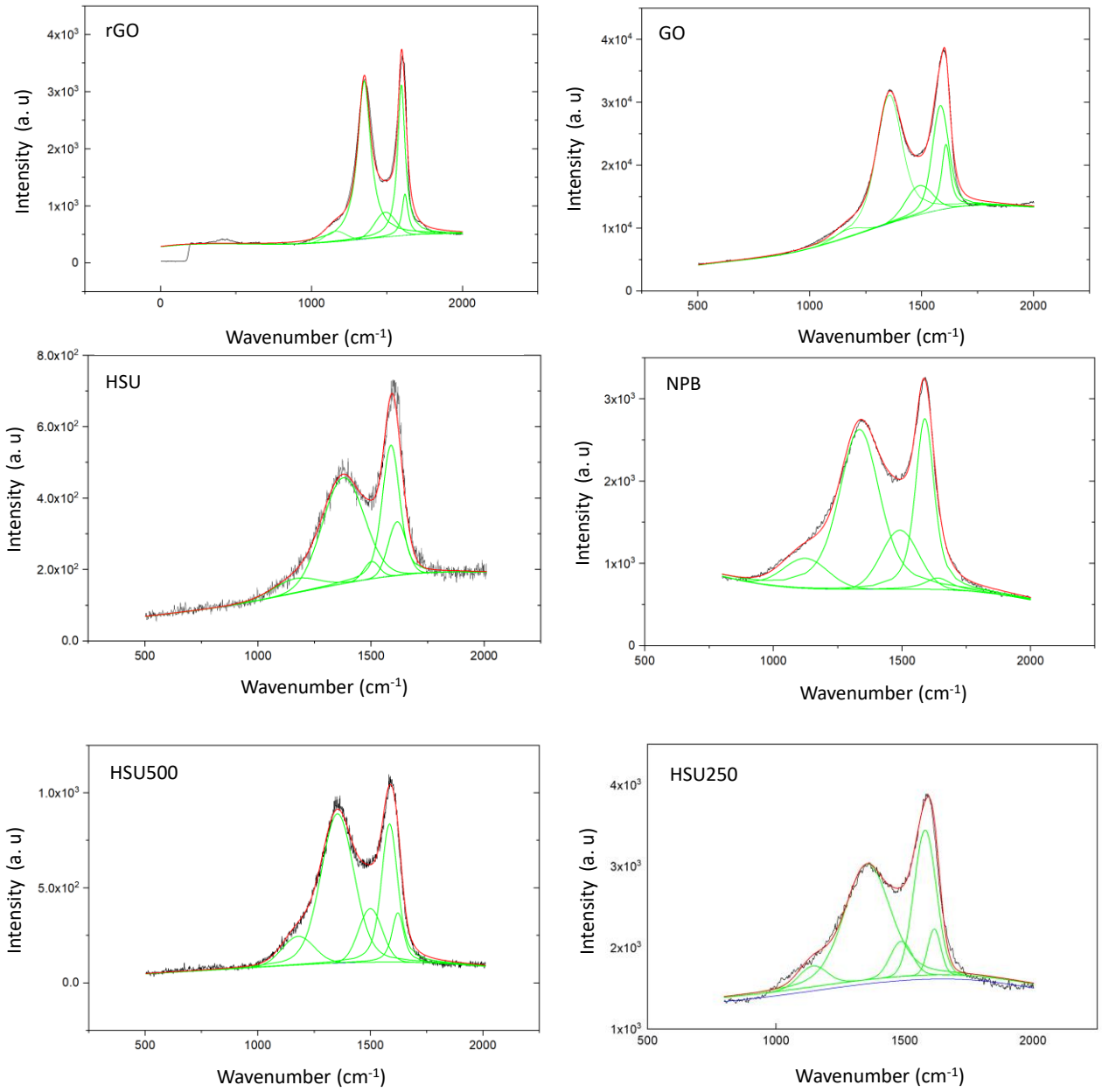

Figure S1. (continued)

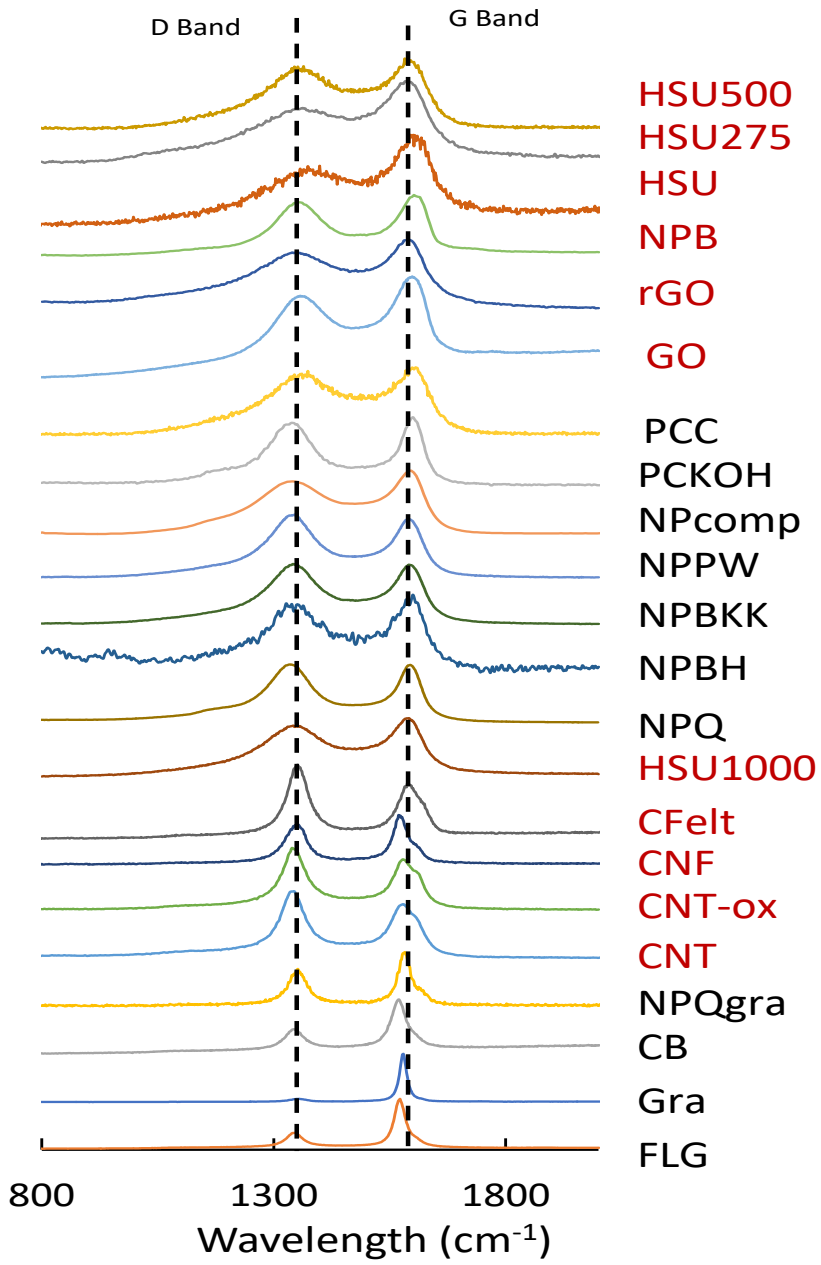

Figure S2. Comparison of the Raman spectra of the studied carbon materials.

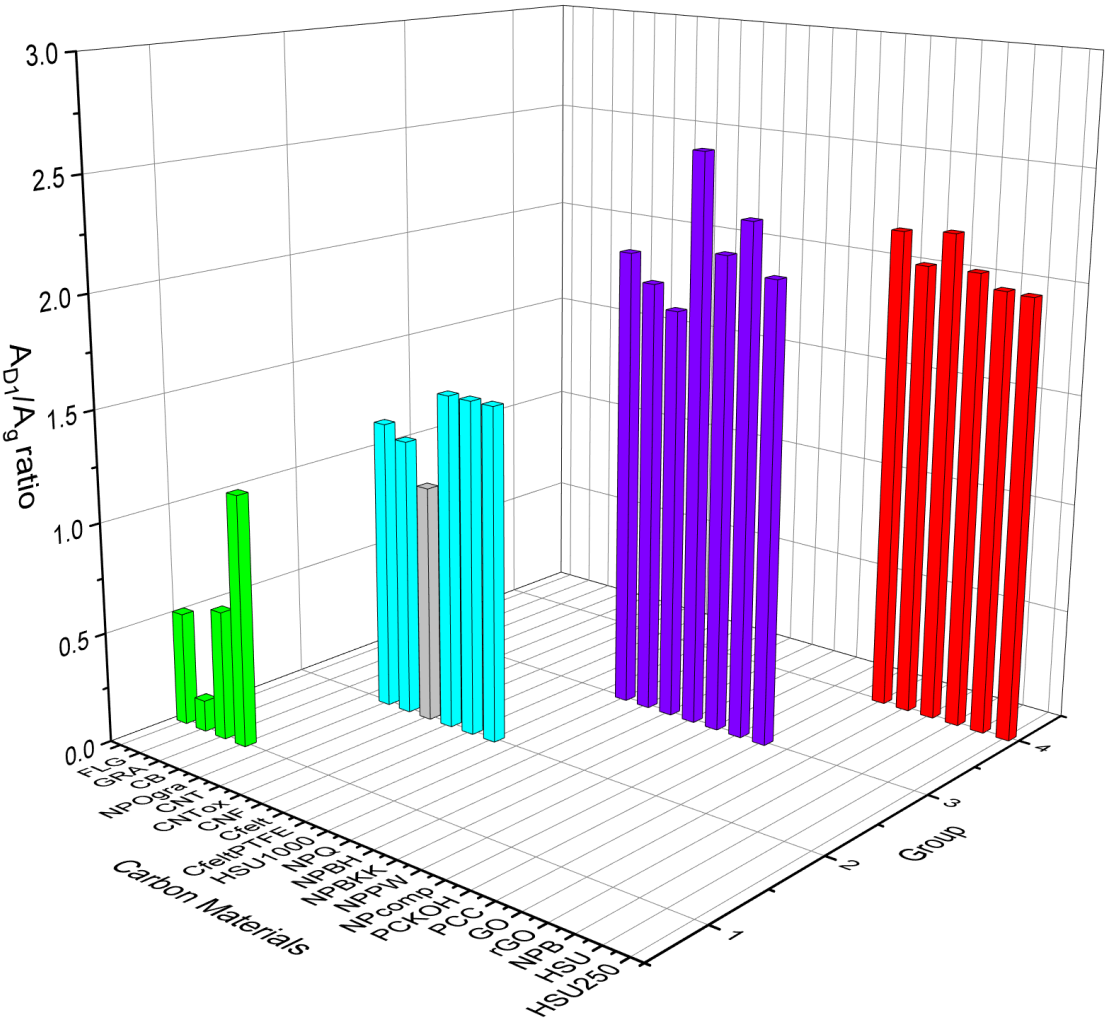

Figure S3. Comparison of the A_{D1}/A_G ratio obtained from the deconvolution of the Raman spectra of the studied carbon materials.

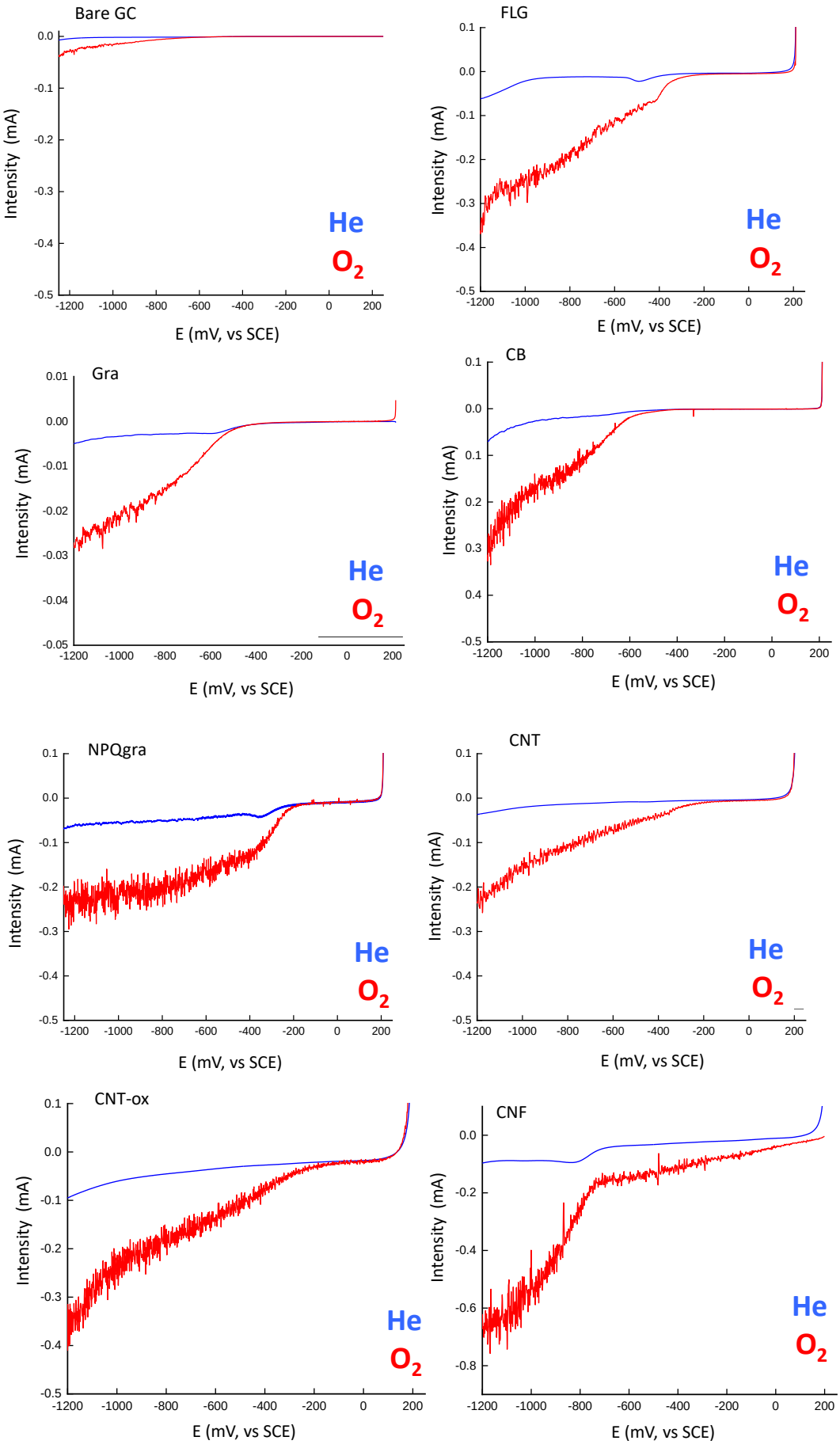
Bare GC
FLG
Gra
CB
NPQgra
CNT
CNT-ox
CNF
Intensity (mA)
E (mV, vs SCE)
He
O2

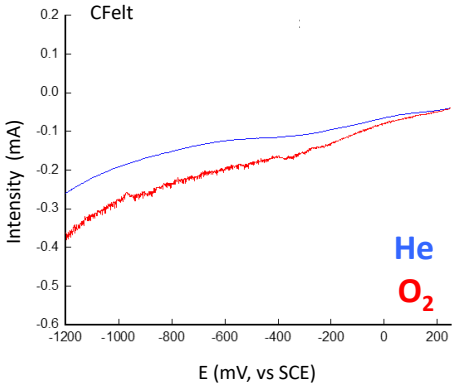
CFelt
Intensity (mA)
E (mV, vs SCE)
He
O2

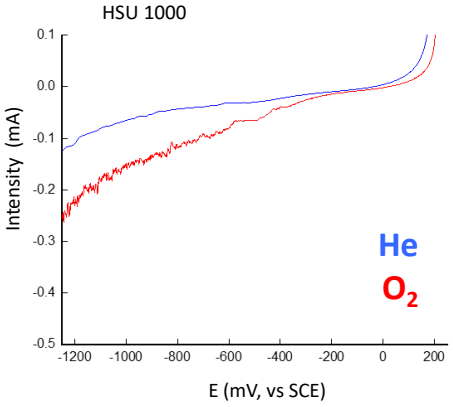
HSU 1000
Intensity (mA)
E (mV, vs SCE)
He
O2

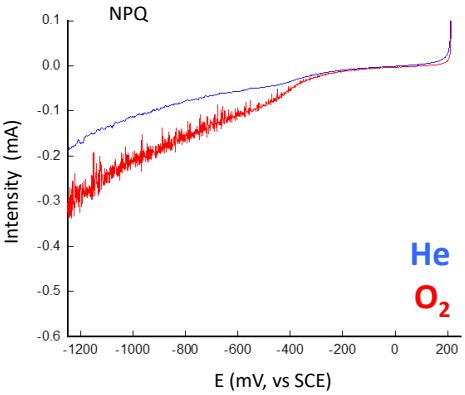
NPQ
Intensity (mA)
E (mV, vs SCE)
He
O2

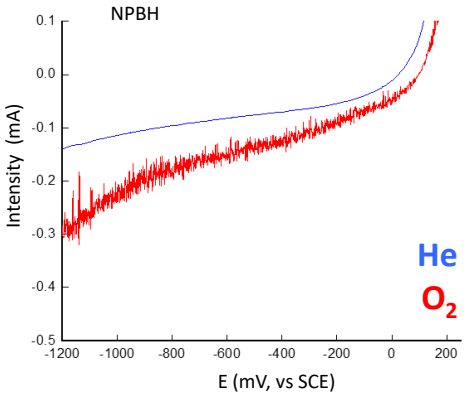
NPBH
Intensity (mA)
E (mV, vs SCE)
He
O2

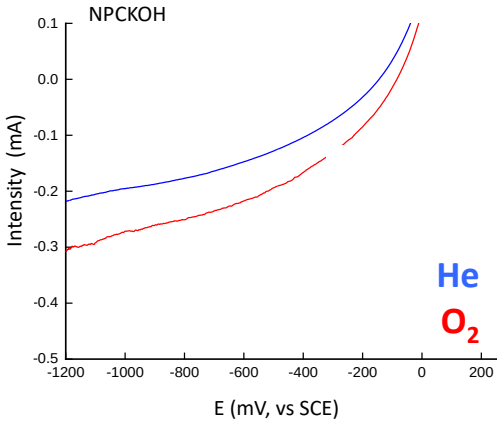
NPCKOH
Intensity (mA)
E (mV, vs SCE)
He
O2

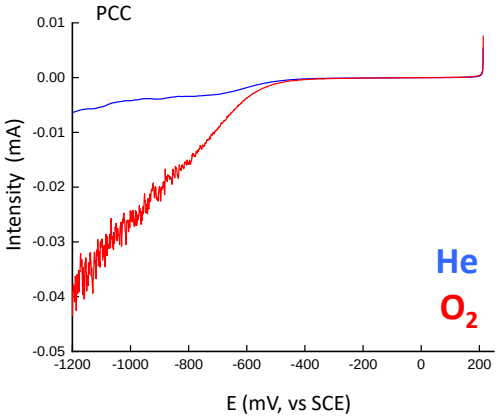
PCC
Intensity (mA)
E (mV, vs SCE)
He
O2

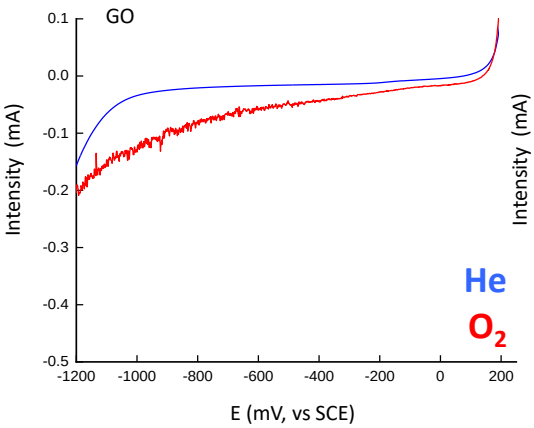
GO
Intensity (mA)
E (mV, vs SCE)
He
O2

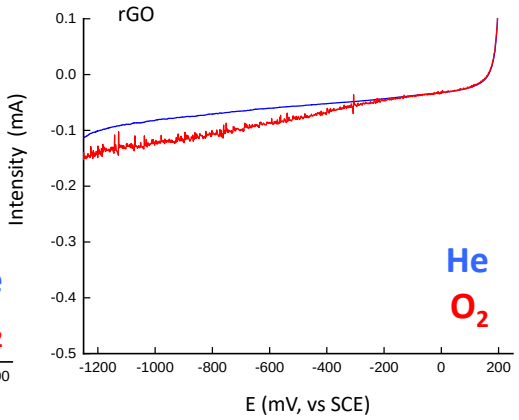
rGO
Intensity (mA)
E (mV, vs SCE)
He
O2

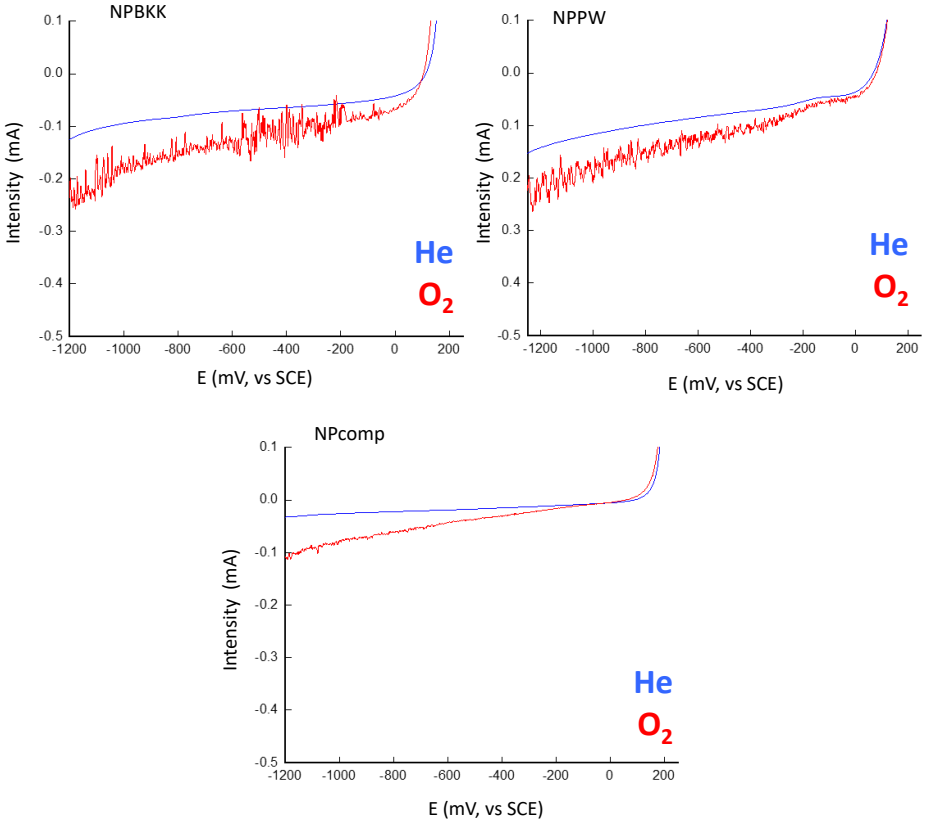
NPBKK
NPPW
NPcomp
Intensity (mA)
E (mV, vs SCE)
He
O2

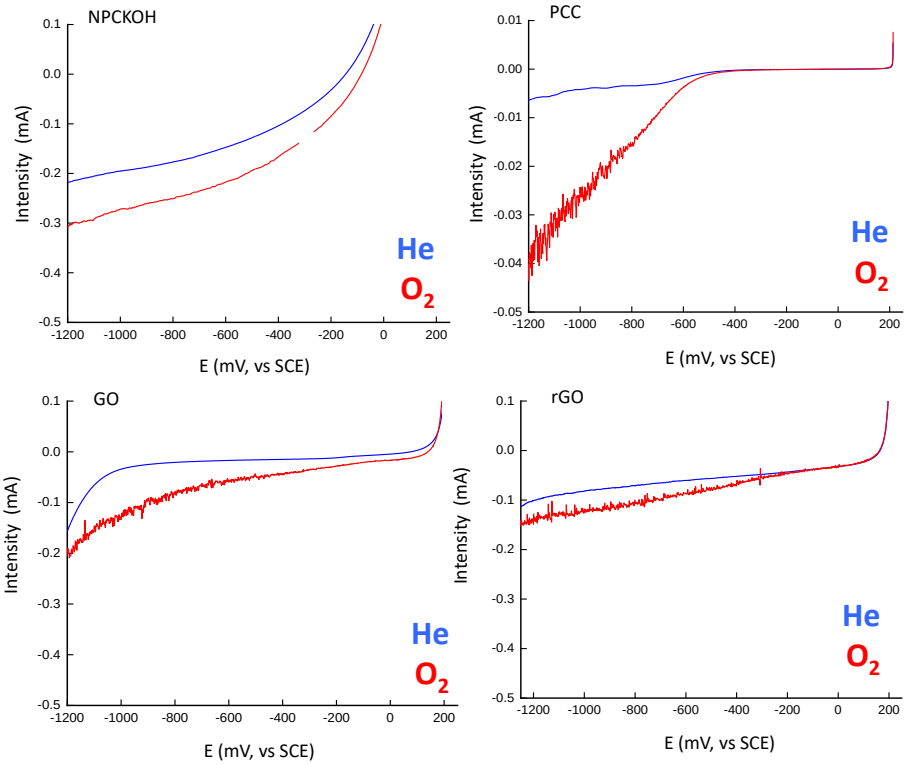
NPCKOH
PCC
GO
rGO
Intensity (mA)
E (mV, vs SCE)
He
O2

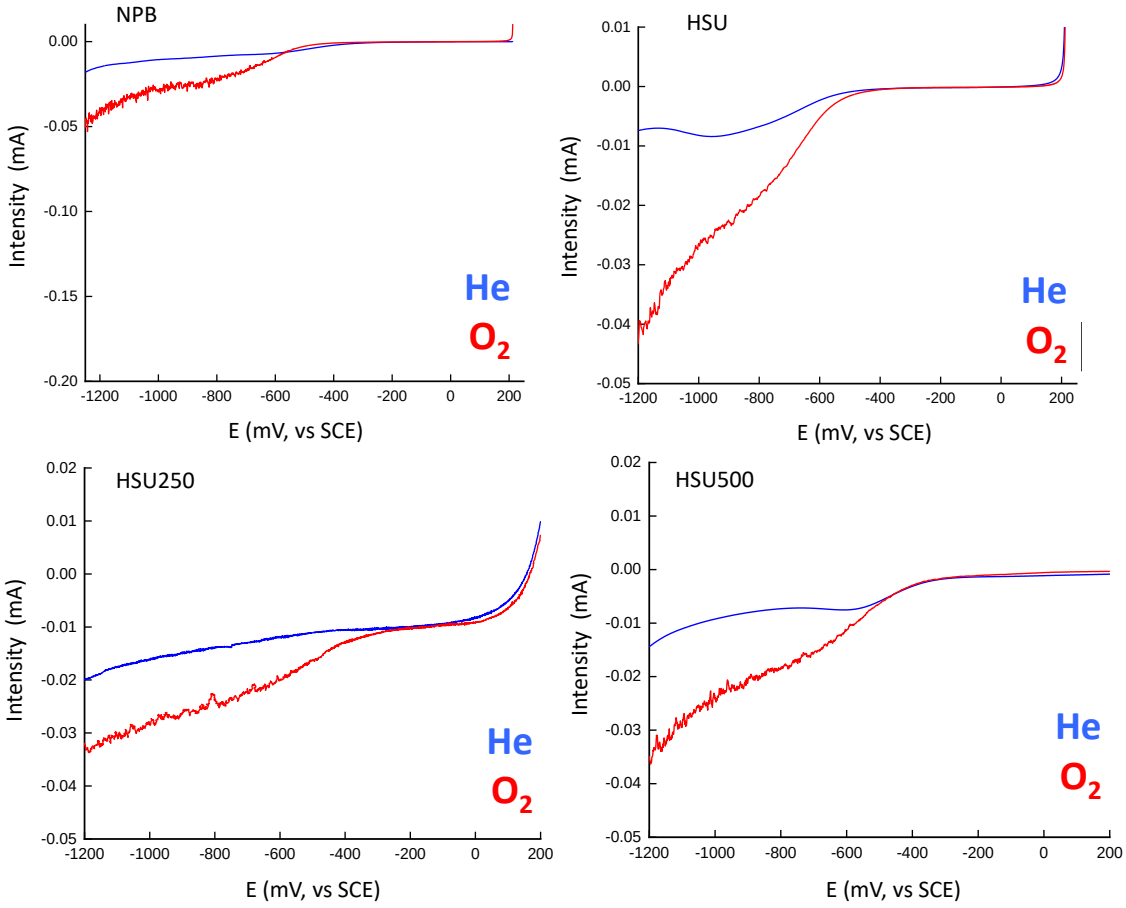

Figure S4. Linear sweep voltametry (LSV) of the studied carbon electrodes using 0.05 M Na_2SO_4 in He-saturated (blue line), and O_2-saturated (green line) stirred conditions. Working electrode: active materials casted on a glassy carbon support (5 mm); counter electrode: Graphite rode; Reference Electrode: saturated calomel (SCE).

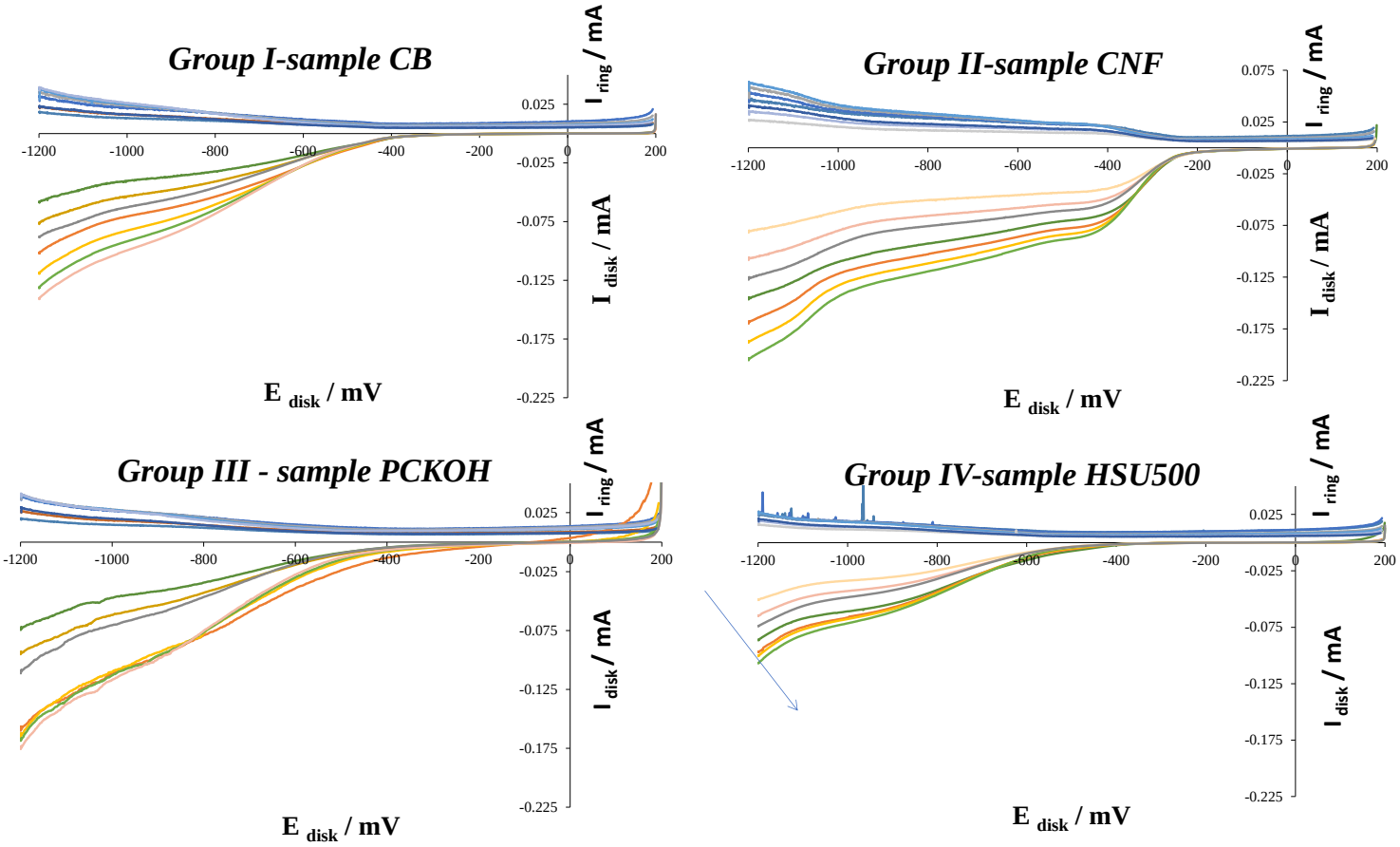

Figure S5. Linear sweep voltammograms for selected studied carbons in O_2-saturated 0.050 M Na_2SO_4 electrolyte using an RRDE, at v_{scan} of 5 mV/s and various rotation speeds (500-5000 rpm). (a) Current of the Pt ring at a E_{ring} of +1.3 V vs Ag/AgCl; (b) current at a glassy carbon disk electrode between 0.2 and -1.3 V vs Ag/AgCl (sweeping towards cathodic values). The catalysts were drop-casted on a 3 mm glassy carbon disk (loading of 0.4 mg/cm^2).

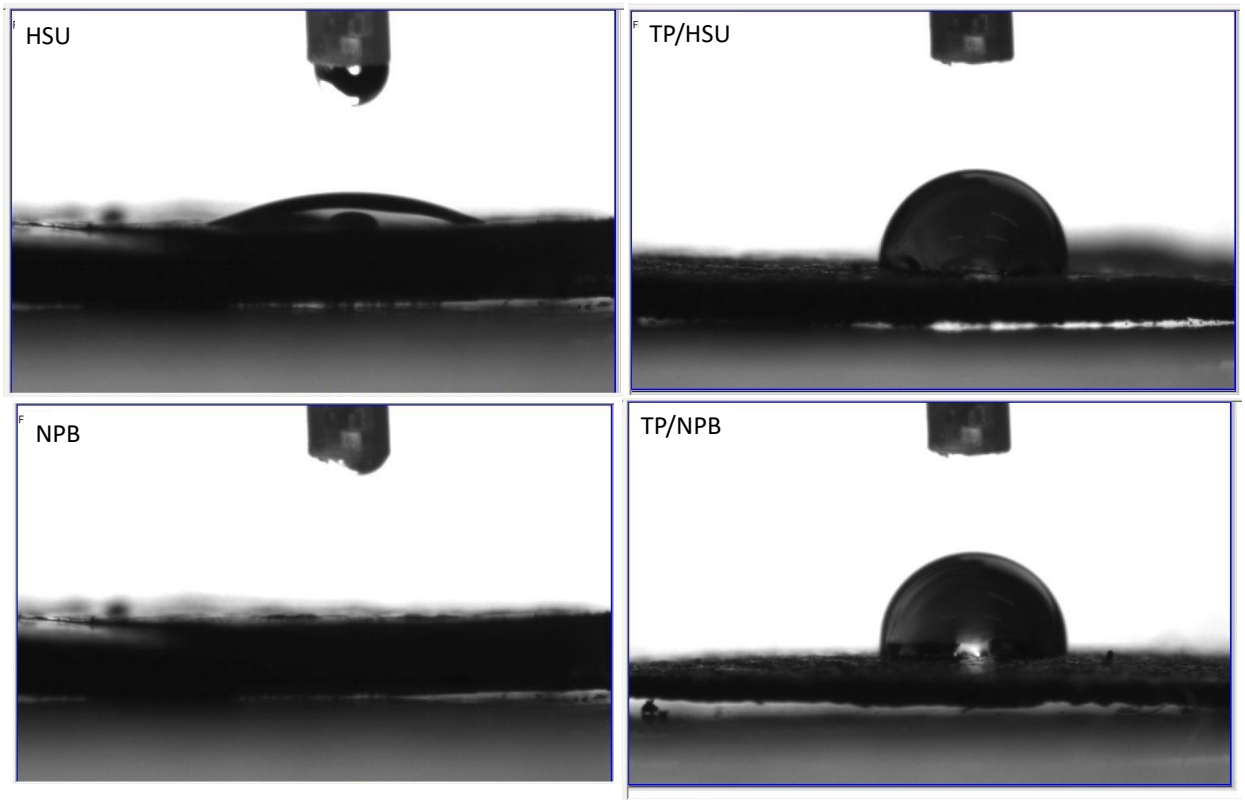

Figure S6. Contact angle measurements for selected hydrophilic carbons (samples HSU and NPB) and their corresponding electrodes (TP/HSU and TP/NPB) prepared from the inks containing 50 mg/mL PTFE binder.

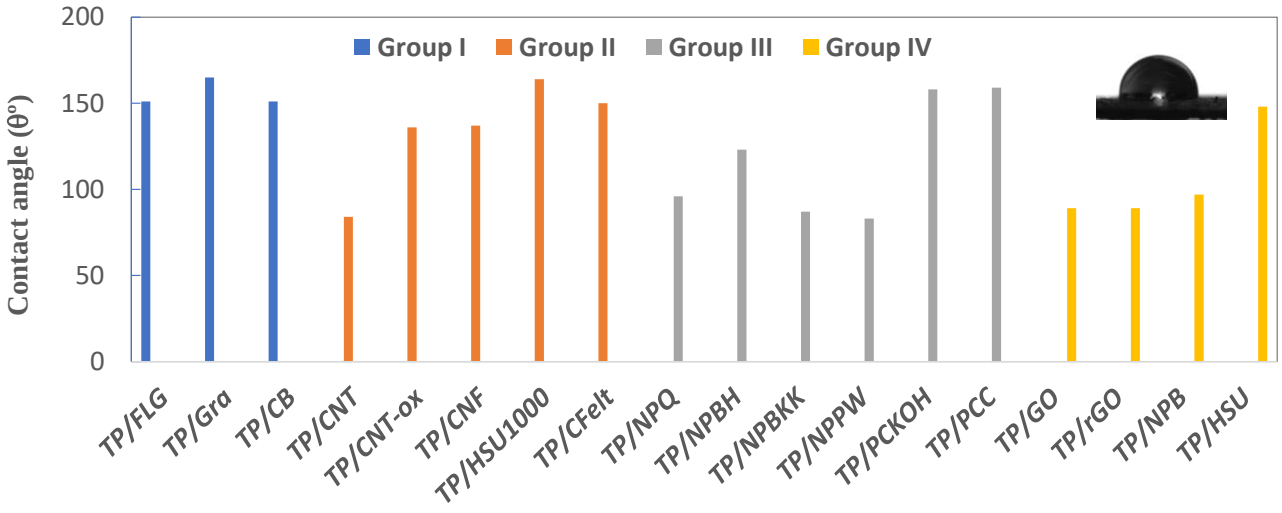

Figure S7. Contact angle of the series of TP/X electrodes prepared with inks of the studied carbon materials containing 50 mg/mL PTFE as binder.

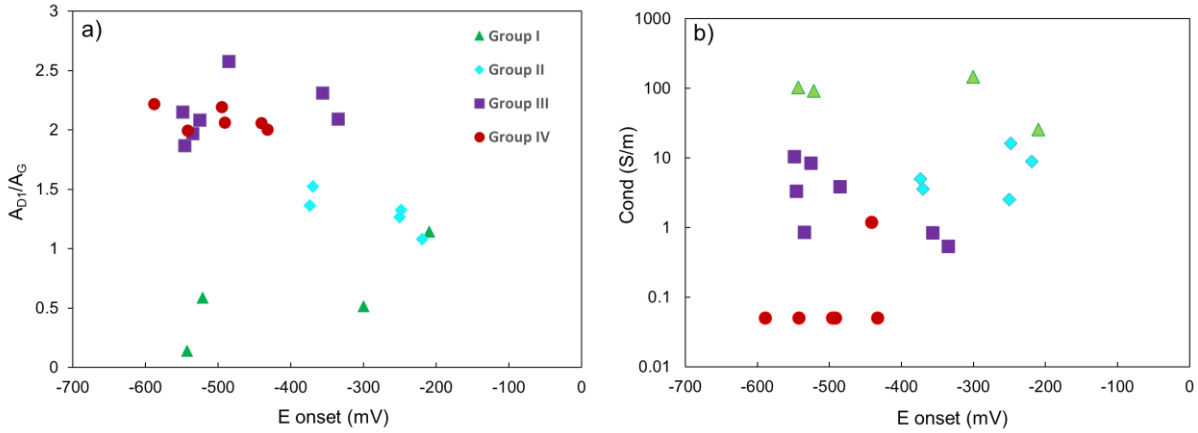

Figure S8. Correlation between the onset potential values and a) the A_{D1}/A_G ratio obtained from the deconvolution of Raman spectra; and b) the electrical conductivity of the studied carbons. Working electrode: glassy carbon (5 mm); counter electrode: graphite rod; reference electrode: saturated calomel (SCE).